Photon detection efficiency measurement of Winston cones for the FAMOUS telescope

von

Johannes Merz

Bachelorarbeit in Physik

vorgelegt der
Fakultät für Mathematik, Informatik und Naturwissenschaften
der
Rheinisch-Westfälischen Technischen Hochschule Aachen

vorgelegt im Juli 2015

angefertigt am

III. Physikalischen Institut A

Erstgutachter und Betreuer

Jun. Prof. Dr. Thomas Bretz
III. Physikalisches Institut A
RWTH Aachen

Zweitgutachter

Prof. Dr. Thomas Hebbeker
III. Physikalisches Institut A
RWTH Aachen

Contents

1. Introduction

For many years cosmic rays have been a central point of interest for particle physicists, as they allow us to learn more about the universe and gather insight to high energy particle physics. Particles, created or accelerated by cosmic events such as supernovae, travel trough our universe and eventually hit the atmosphere of the earth. We call these particles cosmic radiation. They can reach very high energies. It is therefore of high interest for us to study these particles, allowing us to reconstruct their path and learn more about the universe surrounding us [1].

The Pierre Auger observatory, based in Argentina, is a cosmic ray experiment, that utilises a hybrid method to observe these *u*ltra *h*igh *e*nergy *c*osmic *r*ay (UHECR) events. It consists of two main components:

The surface detector (SD) consists of 1660 [1] water tanks, spread across 3000 km^2, arranged in a grid and equipped with three photomultiplier tubes (PMTs) each to detect cherenkov light. This light is created by secondary shower particles originating from the atmosphere. The particles move faster than the speed of light in water when passing trough the water tanks, creating cherenkov light, which is detected by the PMTs.
The fluorescence detector (FD) consists of 27 telescopes located at five different stations overlooking the surface detector. These telescopes detect fluorescence light created in the atmosphere through interaction between the shower particles and nitrogen. The shower axis and spread can be reconstructed, giving valuable information about energy and arrival direction of the cosmic particles.
The fluorescence light in these telescopes is detected trough an aperture system, mirrors, simplified Winston cones (WiCo) and photomultiplier tubes [1].

The *F*irst *A*uger *M*ulti-pixel photon counter camera for the *O*bservation of *U*ltra-high-energy cosmic ray *S*howers (FAMOUS) telescope was born as an idea to improve the Pierre Auger observatory. It looks to utilise silicon photomultipliers (SiPMs) instead of PMTs. At RWTH Aachen University a prototype telescope was developed and constructed. The FAMOUS telescope uses hollow Winston cones to increase the light sensitive area. This thesis looks to examine the cones built for the FAMOUS prototype in an attempt to understand how they influence the telescopes performance and to confirm their viability.

This is done by examining the relative photon detection efficiency (PDE) of a SiPM, that is mounted behind the Winston cone. The PDE indicates how much of the incoming light is detected [2] :

$$PDE = QE \cdot \epsilon_{geom} \cdot \epsilon_{Geiger} \tag{1.1}$$

QE stands for quantum efficiency. It depends on the wavelength of the incoming light and determines the probability for the creation of an electron hole pair in the semiconductors intrinsic area. ϵ_{geom} is the fill factor of the SiPM surface area that is sensible to light. It is set by the production process of the SiPM. ϵ_{Geiger} is the chance for a electron hole pair to create an avalanche. It is highly dependent on the overvoltage $U_{ov} = U_{bias} - U_{breakdown}$ [3].

First off this thesis wants to give a small introduction to the fluorescence light detection. Then briefly explain the working principle of silicon photomultipliers and Winston cones. The experimental setup and the calibration measurements taken are shown. Then follows the main photon detection efficiency measurement of the Winston cones. Finally a conclusion is drawn. The work is evaluated and a small outlook is given.

2. The FAMOUS telescope

2.1 Fluorescence light detection

As introduced before the Pierre Auger observatory measures UHECRs with energies above 10^{17} eV. When such cosmic ray particles, especially atomic nuclei, penetrate the atmosphere of the earth, they interact with molecules in the air. This interaction leads to secondary particles being created, which themselves will hit more molecules and create more particles. This cascade of particles is called an extensive air shower (EAS). This air shower consists of different components, depending on the primary particle. Some particles in this cascade will interact with the nitrogen atoms present in the atmosphere of the earth, which then emit characteristic light.

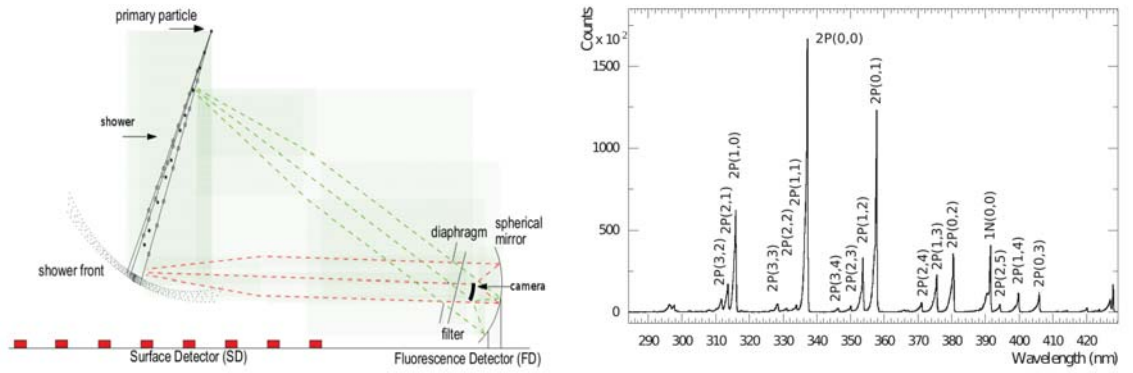

(a) **(b)**

Figure 2.1: a) Schematic of the fluorescence light detection in the Pierre Auger observatory. The primary particle creates the extensive air shower, which emits light. The light is detected by the fluorescence detector of the Pierre Auger observatory. From [3]. b) Fluorescence light of nitrogen corresponding to wavelength. The data has been acquired by the AIRFLY experiment at 800hPa and 293K in dry air, using a 3 MeV electron Beam. From [4].

Fig. 2.1 a) shows a schematic of the fluorescence light detection in the Pierre Auger observatory. The primary shower particle interacts with molecules in the air and creates and extensive air shower. The light emitted by deexiting nitrogen is detected through the optical system of the detectors. Fig. 2.1 b) shows that the dominant transitions correspond to photons with wavelength between 300 and 400 nm. This means that the fluorescence light telescope should ideally be most sensitive in this

spectrum, and as will be shown, SiPMs can provide this characteristic.

2.2 Silicon photomultipliers

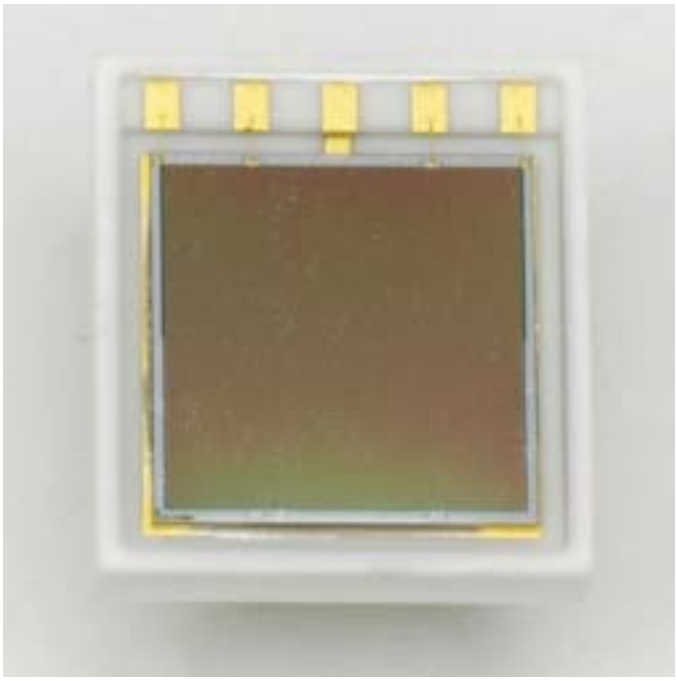

Figure 2.2: The Hamamatsu S10985-100C silicon photomultiplier. From [5]. The SiPM package consists of a ceramic base, the cells and a protective coating. The photo sensitive area is 6x6 mm^2.

But what are SiPMs or silicon photomultipliers? They are semiconductor devices, which, like PMTs, allow for single photon counting.
For a semiconducting material, in our case silicon, to conduct electricity, its electrons have to be excited from the valence band into the conduction band. The semiconducting material is doped with two different materials. One with one more valence electron, creating a free negative charge in the conducting band, and one with one less valence electron, creating a free place in the valence band, a hole. The nucleus of the doping material is locked in the atomic lattice of the silicon, while its additional charge carrier can move. The region doped with a material with an extra valence electron is called n-doped, because it provides negative charge carriers. The region doped with a material with one less electron is called p-doped because the holes in the valence band can be interpreted as positive charge carriers. If the two differently doped regions are brought into direct contact they create a pn-junction [6]. This creates a zone with no free charge carriers, but an intrinsic electric field, the depletion zone. [6]. A voltage, U_{bias} or short U_b, is applied to the outsides of the two zones in such a way, that the depletion zone gets bigger and the intrinsic electric field is amplified.

If a photon, with sufficient energy, now penetrates the semiconductor in this zone, it can excite an electron, in a process called impact ionisation, creating an electron-hole pair. The electron and the hole will be driven by the electric field and moved to the cathode and anode, creating an electric current we can detect, making the pn-junction work as a photodiode.

This effect is used in SiPMs to detect single photons. The voltage across the semiconductor is increased, so that when an electron and a hole are created, they are accelerated and can create secondary electrons and holes in the silicon. This creates an avalanche of electrons and holes, which will increase the measurable electric signal and allow for a reliable way of recognising a photon. The gain, which is the factor, by which the electric signal the photon would create on its own, is amplified, is about 10^5 to 10^6, highly dependent on the overvoltage U_{OV}. The overvoltage is the difference between the bias voltage U_b and the lowest possible voltage that allows an avalanche to be triggered, the so called breakdown voltage $U_{breakdown}$.
If the bias voltage is high enough for a single charge carrier to create a self sustaining avalanche, the semiconductor device is called a Geiger-mode avalanche photo diode (G-APD), similar to a Geiger counter, which also relies on avalanches induced by ionisation through radiation. To limit the current and resulting pulse when an avalanche is triggered, a quenching resistor is connected in series with each photodiode. Due to the current flowing through the quenching resistor in the event of triggered avalanche the bias voltage falls below the breakdown voltage. This prevents the cell, consisting of G-APD and quenching resistor, from being able to detect any more photons. Which in turn will stop the current from flowing through the quenching resistor and make the applied voltage rise again.

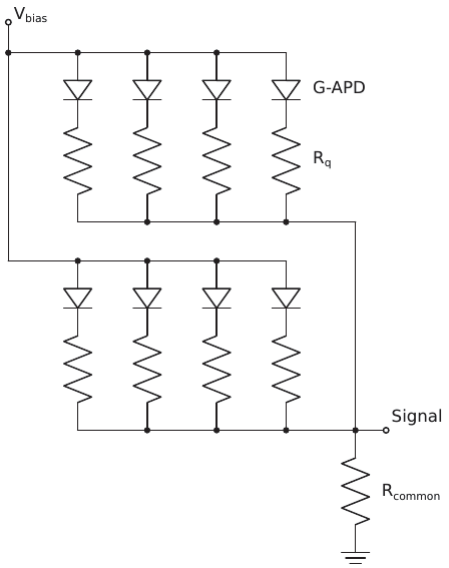

Figure 2.3: Schematic for an array of cells, consisting of G-APD and quenching resistor, wired in parallel. This is the equivalent circuit for a SiPM. The sum of the cells signals is read out over R_{common}. Taken from [4]

To be able to measure a signal proportional to the number of incoming photons, many cells are connected in parallel. This is shown in Fig. 2.3. If a cell triggers current will flow through the diode and the quenching resistor of the cell. If multiple cells trigger the signal at R_{common} is proportional to the number of cells triggered. This is a SiPM.

However a SiPM consisting of such a cell array also has some drawbacks. We will take a look at the three main factors:

Optical crosstalk describes photons, that are created in the avalanche process of a G-APD due to recombination of free carriers, holes and electrons. These photons can cross the borders between cells or travel through the protective coating of the SiPM and create an electron-hole pair in a different cell, triggering an avalanche [3]. This will create a noise signal. Because the distance the crosstalk photons have to travel are so small they trigger additional cells almost instantaneously. This effect will make single p.e. events appear as more p.e. events.

The materials of the SiPM can have small impurities, which will lead to charge carriers getting caught up in the avalanche process and creating a secondary delayed signal with smaller amplitude depending on the amount of voltage across the diode due to cell recovery. This is called afterpulsing.

Thermal noise is the effect of SiPM cells triggering without a photon, but instead by thermal excitation. This effect of course is highly dependent on the temperature. The thermal noise rate of the Hamamatsu SC10985-100C 6x6 mm^2 in the experimental setup was measured and can be seen in Fig. 3.12 on page 23. It is approximately 12 MHz at a trigger level of 0.5 p.e. .

The SiPM only has a limited amount of cells. The dynamic range refers to the range of responding signal to number of incoming photons. If the number of incoming photons, in a small time window, is around the number of cells of the SiPM or higher, the signal measured is not proportional any more. For a very high light intensity the SiPM response saturates.

The SiPM used in this thesis is the Hamamatsu MPPC S10985-100C, shown in Fig. 2.2. It has a photosensitive area of 6x6 mm^2. It consists of 3600 cells with cell pitch of 100 μm. Its spectral response ranges from 320 nm to 900 nm. It reaches its peak PDE around 400 nm [5]. The operation voltage for the specific SiPM used in the experiment, was given by Hamamatsu at 70.81 V.

The cells of the SiPM are protected by a coating. The coating provides good mechanical protection. Numerous times during the work on this thesis the durability of SiPMs could be confirmed. This coating has a different refractive index than air. The SiPM's performance depends on the entrance angle of light to the surface. D. Wilson researched this effect in his bachelor thesis [7].

The angular dependence found for the Hamamatsu S103612-11-100C SiPM shown in Fig. 2.4 will be used.

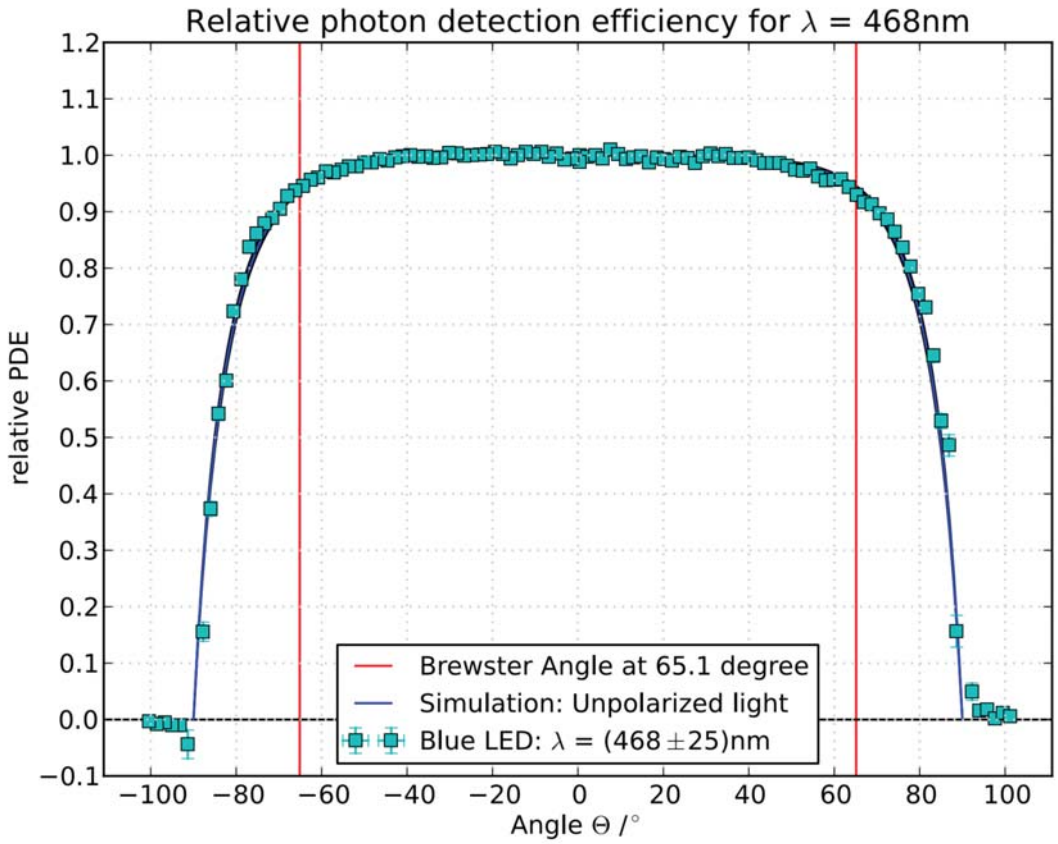

Figure 2.4: The angular photon detection efficiency for the Hamamatsu S103612-11-100C SiPM found by D. Wilson [7]. The S103612-11-100C offers similar properties as the S10985-100C.

2.3 Winston cones

Winston cones are light concentrators highly suitable for telescopes as they offer very high transmission efficiencies [8] and a limited field of view, cutting out possible scattered light. Furthermore they can be designed hollow, minimising the material put in the path of the light and therefore minimising possible absorption, especially in the UV spectrum of the fluorescence light.

Winston cones are designed by defining two of three parameters: The exit aperture r_2, the entrance aperture r_1 and the maximal acceptance angle θ_{max}. Given the entrance and exit aperture we can follow a light ray, starting at distance r_1 to the optical axis, that enters the cone at θ_{max}. The parabola of the cone is designed in such a way that the light focuses in a point at the end of the cone with distance r_2 to the optical axis, like pictured in Fig. 2.5.
It is clear that the Winston cone therefore is described by two parameters already:

$$\sin\theta_{max} = \frac{r_2}{r_1} \tag{2.1}$$

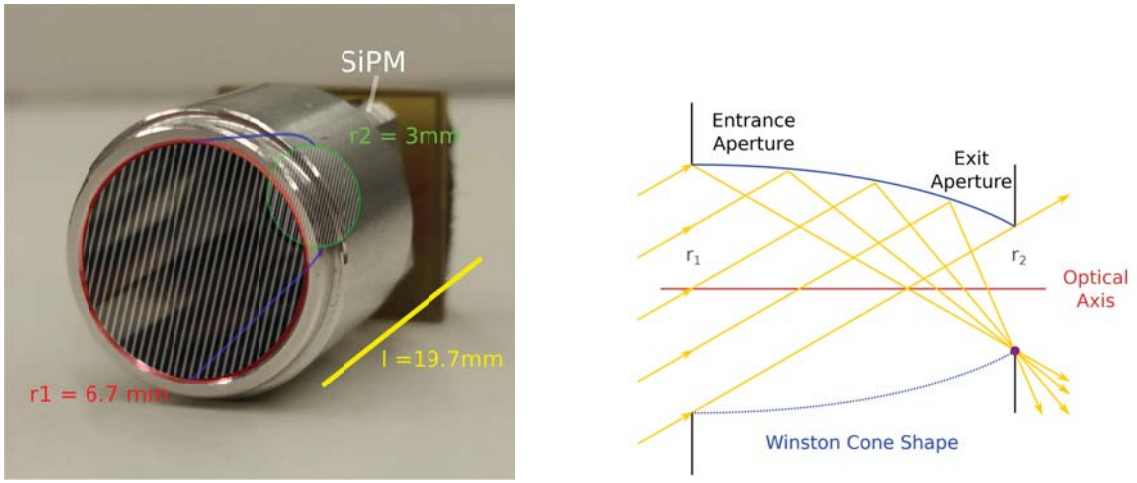

(a) **(b)**

Figure 2.5: a) A picture of the FAMOUS Winston cone used in the experiment. As explained the SiPM is glued in the notch at the end of the cone. The small circuit board, seen at the end of the cone in a), has two contacts that allow to easily supply the bis voltage to the SiPM. The construction parameters are highlighted. The entrance aperture in red with a radius r1 = 6.7 mm and the exit aperture in green with a radius of 3 mm. b) Schematics taken from [4] showing the construction principle of a Winston cone.

The length of the Winston cone follows as:

$$l = \frac{r_1 + r_2}{\tan \theta_{max}} \tag{2.2}$$

Combining equations (2.1) and (2.2) we can fully describe the Winston cone parabola [8]:

$$r(\theta) = \frac{1 + \sin \theta_{max}}{1 - \cos(\theta + \theta_{max})} 2r_2 \tag{2.3}$$

This is shown in 2.6, including the parameters chosen for the Winston cones used in the FAMOUS telescope:

$$r_1 = 6.71\,\text{mm} \tag{2.4}$$

$$r_2 = 3.00\,\text{mm} \tag{2.5}$$

$$\theta_{max} = 26.6^\circ \tag{2.6}$$

$$l = 19.6\,\text{mm} \tag{2.7}$$

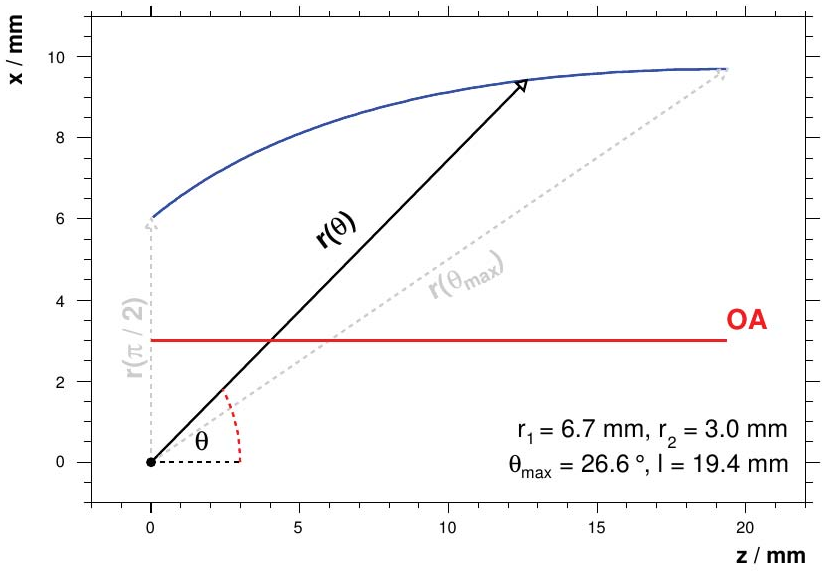

Figure 2.6: The Definition of the Winston cone Parabola. We see that the reference point is the focal point of θ_{max}. The parameters given are the ones used for the FAMOUS Winston cones. From [4]

Because of the parabolic shape, the light, if reflected, exits the cone with increased angles. This means, the cone does not preserve the image information and is therefore called a non-imaging device [8].
A simulation of a two dimensional Winston cone was written in Matlab 2014b to understand how the exit angle of the light shifts with changing entrance angle. We see in Fig 2.7 the exit angles broaden for higher entrance angles.

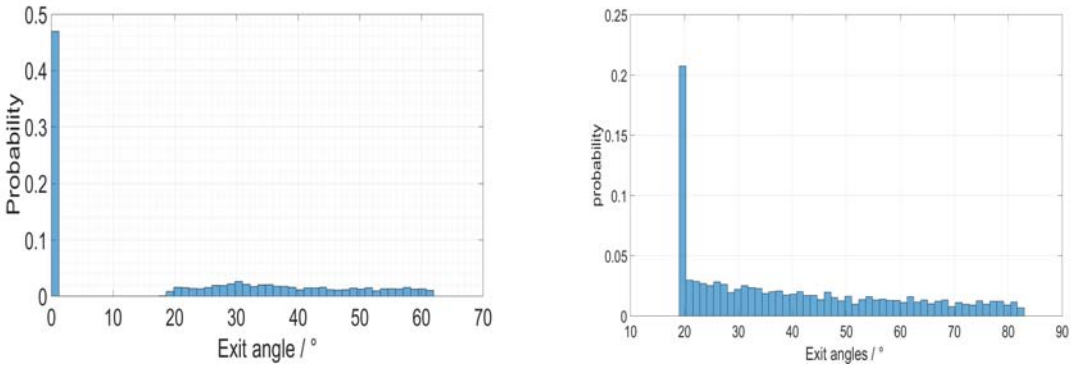

(a) **(b)**

Figure 2.7: These histograms show the exit angle of the light with a) 0° entrance angle and b) 20° degrees entrance angle for 5000 simulated photons respectively

The strong point of Winston cones is their transmission. While the light sensitive area is increased to almost four times the size of the SiPM, light is only lost due the

reflectivity of the material used for the cones. For the FAMOUS Winston cones polished aluminium is used. It decreases the transmission efficiency slightly, compared to a perfect Winston cone. For the simulation a reflectivity of 0.94 was chosen in accordance to the data described in [9].

The lobed surface of the machined aluminium also slightly broadens the possible exit angles of the Winston cone as found by the simulations from T. Niggemann in[4].

2.4 The FAMOUS telescope prototype

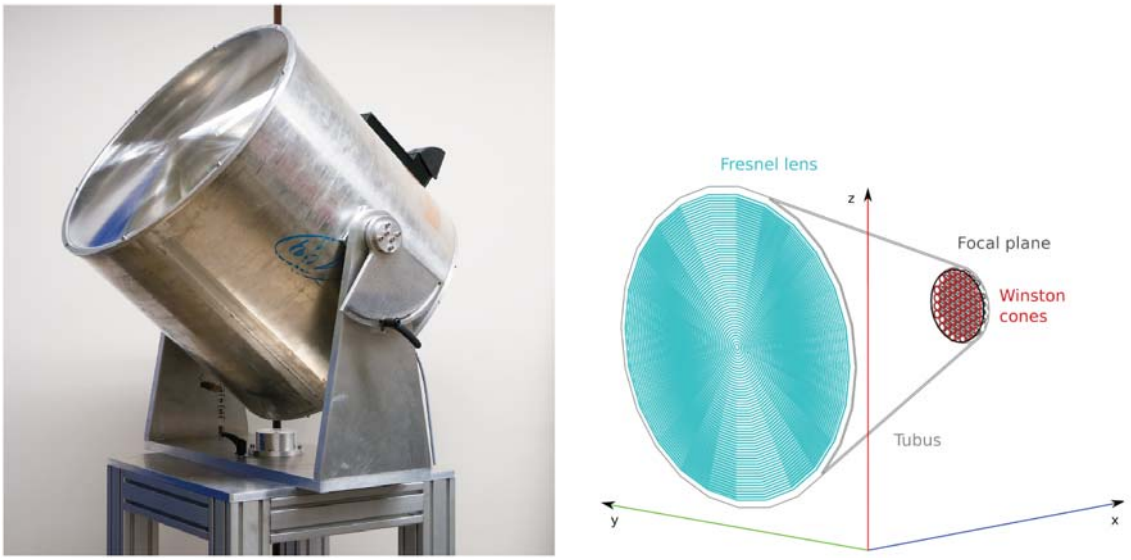

(a) **(b)**

Figure 2.8: a) Picture of the FAMOUS^{SEVEN} prototype fully assembled. Taken from [10]. b) A schematic of the optical system of the FAMOUS telescope. It shows the Fresnel lens that focuses light on the focal plane. Each Winston cone on the focal plane concentrates the light onto a SiPM. Made in Geant4 by [4].

The FAMOUS telescope consists of a Fresnel lens focusing the incoming light on a focal plane with 61 Winston cones. Each Winston cone directs the light on a separate SiPM. We can see the design of the optical system in figure 2.8 b).

The FAMOUS^{SEVEN} prototype has been fully operational and can be seen in Fig. 2.8 a). It only uses 7 SiPMs and Winston cones on its focal plane of type Hamamatsu S10985-100C. The Winston cones use the same parameters as mentioned above.

The following measurements in this thesis have been made with the Winston cones of the FAMOUS^{SEVEN} prototype. They were machined by the Mechanical Workshop of III. Physikalisches Institut A, RWTH Aachen University. The Winston cones for the 61 pixel version of FAMOUS will have the same parameters but thinner walls,

decreasing the dead space between the pixels. However, this has hardly any influence on the performance of the cone since the parameters, r1, r2, θ_{max} are the same for both Winston cones. The new version of FAMOUS will also utilise newer SiPMs with better photon detection efficiency and lowered correlated noise effects, especially afterpulsing.

3. Experimental setup and calibration measurements

3.1 Experimental setup

The goal is to perform a relative photon detection efficiency measurement in dependency of the entrance angle θ of the light.

To realise an angular dependent photon detection efficiency measurement a few key elements have to be considered: The light leaving the cone has to be measured. Naturally one of Hamamatsu S10985-100C, used by FAMOUS, was chosen. The light source should illuminate the whole cone evenly and homogeneously with parallel pulsed light. For an automated measurement the cone needs to be rotated automatically. The SiPM pulses have to be read and computed. The experimental setup should be shielded from external light sources.
These conditions were met in the setup shown in Fig.3.1.

The base plate and holding parts for the experiment were from the Thorlabs optical experiment series. They allowed for a solid base and an easy way of aligning the optical parts. They were placed inside a dark box lined with black felt on the inside to minimise scattering light. The temperature in the room where the experiments were performed kept constant by a air conditioning system. This was especially useful in regards to the temperature dependent gain of the SiPM.
The Winston cone was fitted in an aluminium mounting, which was commissioned to the mechanical workshop of III. Physikalisches Institute A of the RWTH Aachen university. The mounting allowed the cone to be fastened with small screws and was designed in such a way, that the cone's entrance could be rotated on the optical axis, as shown in Fig. 3.1 and in Fig. 3.2.

The rotation was realised by a stepper motor. The SY35ST28-0504A, a hybrid bipolar stepper motor with 200 steps per revolution. It is connected to an arduino uno micro controller board, which allows for double coil movement, increasing the steps per revolution to 400. This will be verified through calibration measurements. An arduino program allowed for communication with the micro controller through the serial interface. Making it possible to send commands for stepping, while keeping count of the steps and allowing to return to the starting position.
Mounting the SiPM to the end of the cone proved to show some difficulties. Early

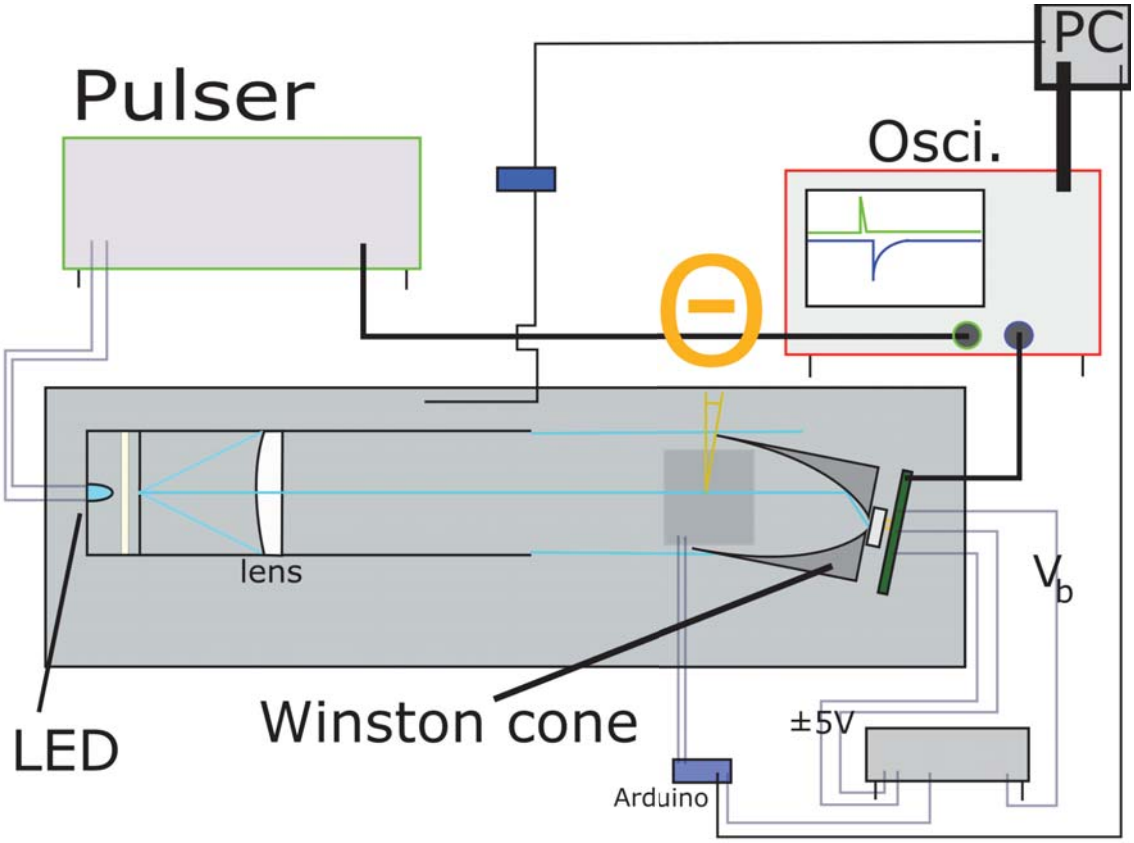

Figure 3.1: The experimental setup for the photon detection efficiency measurement. The Winston cone and SiPM are placed in a dark box, that shields them from external light. With the Thorlabs optical experiment parts the optical system consisting of a pulsed LED, a piece of sandwich paper as a diffuser and a spherical lens were mounted in the optical axis of the cone. The cone itself is mounted in an aluminium mounting on a stepper motor, allowing it to rotate with its entrance centred on the optical axis. The SiPM and the arduino driving the Motor are powered by a power supply. The SiPM sends it signal to the oscilloscope to be measured and send to the computer for evaluation. The arduino controlling the motor also communicates with the computer via a serial interface. An extra arduino controls a temperature sensor for monitoring.

measurements were performed with small clamps constructed of metal wire. Because of the front end electronic they could not provide enough pressure evenly on the SiPM. This created an unsymmetrical gap between the end of the cone and the top of the SiPM resulting in huge angular errors. See appendix Fig. A.1 and Fig. A.2. To fix these problems the SiPM was glued in the notch at the end of the Winston cone. Great effort was made to keep any glue from leaking on the front side of the SiPM, creating a gap or disturbing the path of the light. In the FAMOUS telescope an additional filter plate is mounted in the notch of the cone. Which will prevent such problems.
The SiPM is supplied with the bias voltage U_b, the other voltage of ±5V is sup-

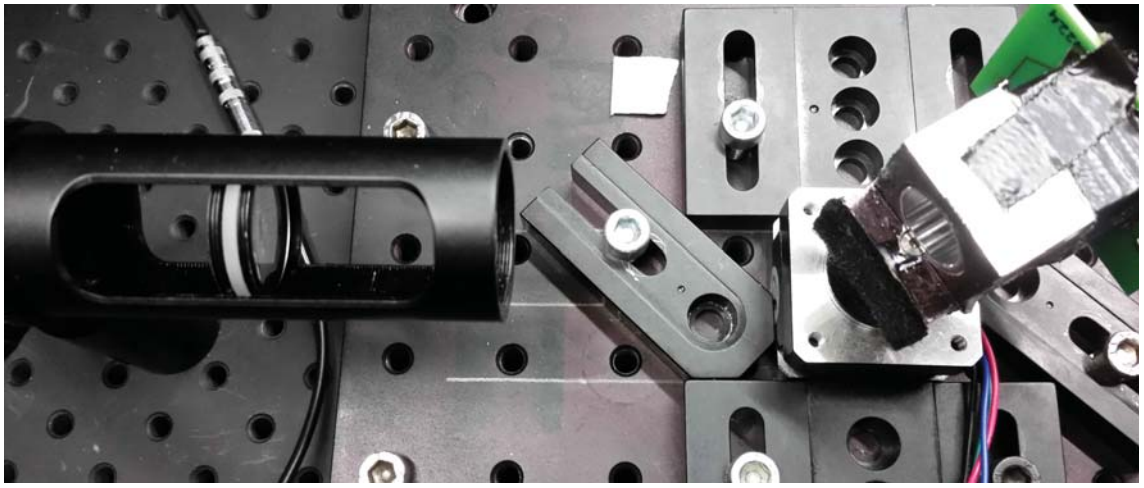

Figure 3.2: The Winston cone in the aluminium mounting in front of the light source. It rotates with the center of the entrance aperture on the optical axis.

plied to the front end electronic by the powersupply. The front end electronic was designed by J. Schumacher. The design process is explained in [11]. This electronic was designed especially for dynamic range measurements utilising a small gain resistor to allow for high SiPM pulses without saturation of the op-amp. It consists most importantly of an operational amplifier and a low-ohmic low pass on the U_b line.

The operational amplifier on the front-end board amplifies the SiPM signal, which is digitised by the oscilloscope, a LeCroy WaveJet 354A. The oscilloscope also receives the output signal of the pulse generator, a Hewlett Packard 8082A pulse generator, which powers the light source, a sanded LED with $\lambda = 397\,\text{nm}$. This allows the oscilloscope to trigger on the pulses and measure the responding pulse the SiPM sees. We can see a screenshot as an example of this process in Fig. 3.3.

The oscilloscope digitises the SiPM signal with 500 points per 500 ns, or 1 GS. This amount of sample points was chosen for the calculated integral to be accurate. The measurement mechanic of the oscilloscope only allowed for two measurements per second. This resulted in long measurement times if many pulse signals were to be measured to gain enough statistic. The oscilloscope is connected to the computer and, after integrating the pulses over $\Delta t = 215\,\text{ns}$, transmits the measured integral values. $\Delta t = 215\,\text{ns}$ was chosen so that even for very high light intensities 90% of the pulse was integrated.

The pulser drives the light source. A sanded LED with $\lambda = 397\,\text{nm}$. The power required to drive the LED was determined by having the cone and SiPM face the light source at $\theta = 0°$. The voltage was lowered until the SiPM signal was quite a bit under the saturation. This was done to stay in the linear part of the SiPM's dynamic range. The LED voltage was $3.4 \pm 0.1\,\text{V}$. A sanded LED was chosen as the light source after some considerations, which will be discussed later. The LED is mounted with the Thorlabs system. Therefore it is centred in the optical system, as seen in 3.4 a). Directly behind the LED a piece of sandwich paper is installed, see

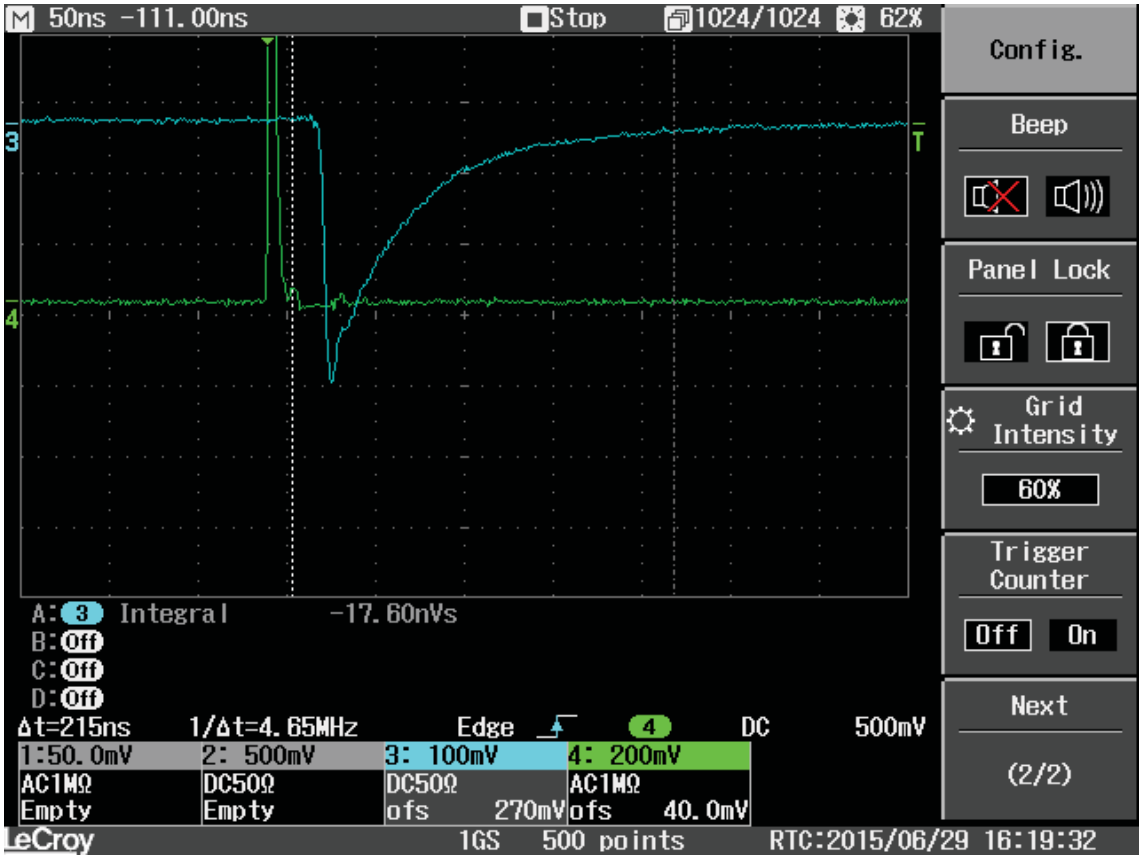

Figure 3.3: A screenshot of the oscilloscope. We see the output signal of the pulse generator in green and the responding SiPM signal in blue. The oscilloscope directly performs a measurement integrating over the shown time $\Delta t = 215\,\text{ns}$. The angle θ is 15°.

3.4 b). It was chosen to make the emitting light as homogeneous as possible. With some very small distance the pinhole aperture, see 3.4 c), is mounted next. It is of great importance as it allows the light source to be approximated as a point source. With an ideal point source the lens would create parallel light, but as the pinhole has a small diameter of approximately 0.3 mm the lens can hardly create parallel light. This and the fact, that due to the mounting system the light source has some distance from the pinhole, will make it challenging to achieve parallel light.

After the pinhole a lens tube, a Thorlabs SM1L30C, is screwed to the other parts. It allows to move the lens, which is clamped between two retaining rings, Thorlabs SM1RR (diameter 1 inch), while supplying a sturdy hold. The lens is a Thorlabs LA1422 N-BK7 spherical plano-convex glass lens, with a diameter of 1 inch. This way the lens is positioned for the pinhole to lay in its focal point at 40.0 mm. The lens should make the light parallel, but includes some errors among other due to its spherical nature. We will see this effect later.

A C++ program was written that controls the stepper motor and oscilloscope data readout. With this a relative PDE measurement can be performed. The motor, con-

(a) (b) (c)

Figure 3.4: The sanded down LED. Sandwich paper used as a diffusor, mounted in a Thorlabs ring system. The pinhole aperture.

trolled by the program, rotates the Winston cone and SiPM, while the LED sends light pulses on the cone. The oscilloscope triggers on the pulses and reads out the answering SiPM signal, which is integrated. The integral values are forwarded to the pc, where they are stored and the mean and standard deviation are calculated. The integral values are normalised to the value measured at $\theta = 0°$. This plotted in regards to the entrance angle θ finishes the PDE measurement.

3.2 Validation of experimental setup and calibration measurements

3.2.1 Different light sources

Before real measurements were performed, different light sources were inspected for their viability. This was done using a Alccd-QHY 5L-II-c camera. The camera was put directly at the end of the lens tube. The CCD sensor was too small to fit the whole illuminated area.
The three different light sources were a normal LED, with $\lambda = 397\,\text{nm}$, a LED sanded down with fine grit, also $\lambda = 397\,\text{nm}$, and the integrating sphere, which was illuminated with the normal LED. In case of the integrating sphere the optical fibre, used to guide the light, was hold by hand. For these measurements the sandwich paper was not yet installed.
First up is the normal LED. Pictures are taken with the camera at the end of the lens tube. In Fig. 3.5 we see that the normal LED is very inhomogeneous and would in no way be suitable to perform the experiment, as the light intensity varies heavily.

The light leaving the optical system wit the sanded down LED installed can be seen in Fig. 3.6. It was sanded with fine grit sanding paper. The bright illuminated bezel is due to the aforementioned lens errors, such us spherical aberration. The diameter of the lens is 1 inch. The retaining rings, holding the lens, reduce this diameter by 4 mm. The retaining rings can be see in 3.2. This leaves 10.7 mm

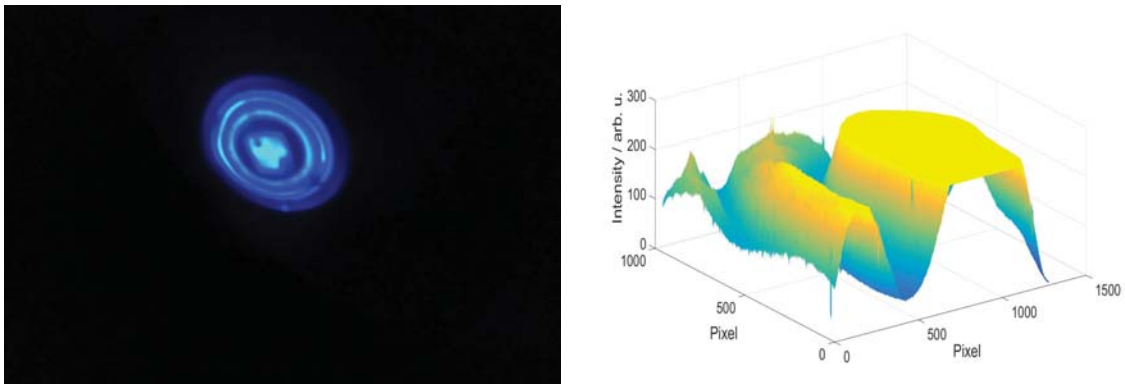

(a) **(b)**

Figure 3.5: a) Photo of the light leaving the lens with the normal LED as a light source. b) The light intensity that the CCD camera sees plotted. It is only a segment of the full illuminated area.

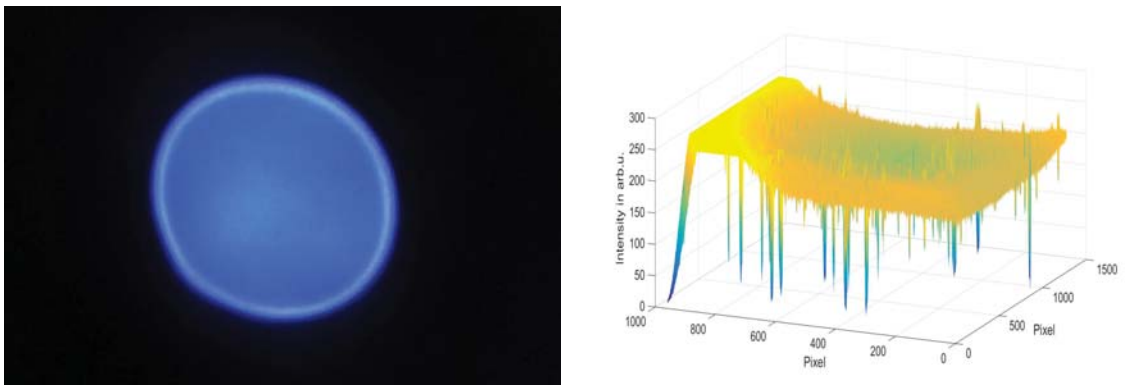

(a) **(b)**

Figure 3.6: a) Photo of the light leaving the lens with the sanded LED as a light source. b) The light intensities for a of center segment of the illuminated area. The inhomogeneity inside the bezel is greatly reduced compared to the normal LED. The bright bezel is far more intense than the center segment. It reduces the area suitable to illuminate the cone homogeneously.

radius for the illuminated ring, compared to the 6.7 mm entrance aperture of the Winston cone. The lens error further reduces the homogeneously illuminated radius by approximately 2 mm. Leaving only 8.7 mm radius for the illuminated area right at the end of the lens tube.
Although the sanded LED offers increased homogeneity, Fig. 3.6 still shows that the center of the illuminated area is not lit very homogeneously.

The integrating sphere absorbs a lot of the intensity, as we can see in Fig. 3.7, as the light is much weaker. We can still see the effect of lens errors in the photo in 3.7. The intensities measured by the CCD sensor vary a lot, because of the low intensity.

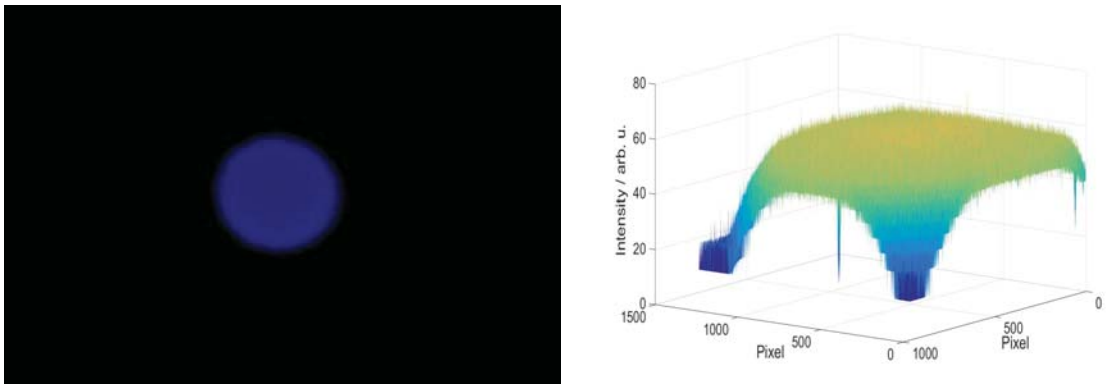

(a) (b)

Figure 3.7: a) Light leaving the lens with the integrating sphere as the light source. b) Plot of the light intensities . Because the intensity is so low the digitalisation of of the CCD camera becomes visible.

The sanded LED seems to be a viable alternative to the integrating sphere, in the sense that the huge inhomogeneities could be drastically reduced. Further efforts are made to decrease the inhomogeneities.

3.2.2 Homogeneity

Now a series of pictures was taken with varying distances between the end of the lens tube and the CCD camera. The sanded LED is used as the light source. The sandwich paper is not yet installed.

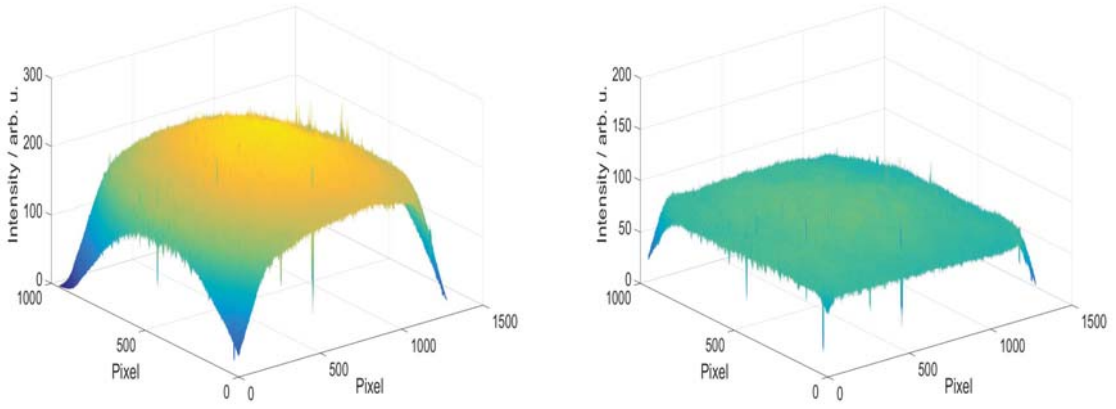

(a) (b)

Figure 3.8: Intensity plots of CCD pictures. Taken in a distance of a) 6mm and b) 151mm from the lens tube.

Two of these measurements are shown in Fig. 3.8. It is clearly visible that the light gets more homogeneous with increasing distance. For this measurements a lens system is installed in front of the CCD sensor, that allowed to zoom in on the center

parts of the illuminated, shutting out the bright bezel. Because the light in this bezel is not parallel it widens with increasing distance.

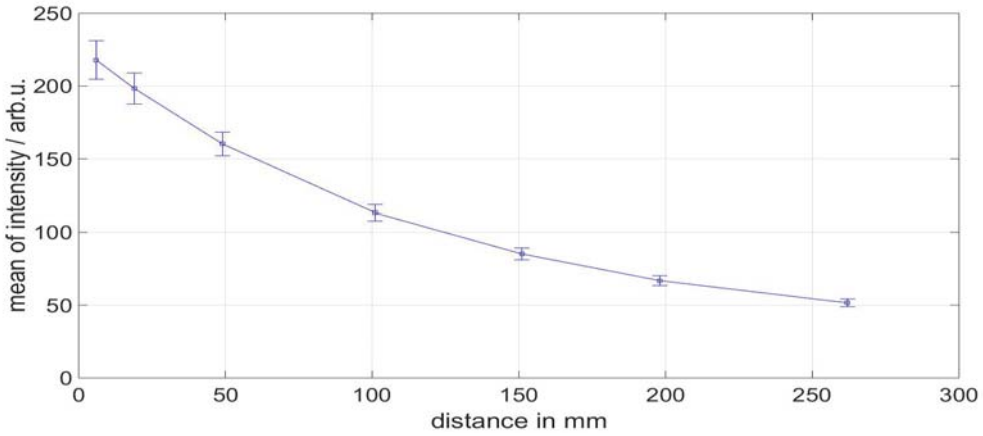

Figure 3.9: Mean intensities seen by the CCD camera at different distances. The error is the standard deviation. The light source was the sanded LED. The sandwich paper was not yet installed.

The plot in Fig. 3.9 shows clearly that the relative error decreases significantly with increasing distance. In conclusion the cone should be positioned with as much distance as possible. However the bright bezel, due to the nature of the lens, scattered more with increasing distance, making it impossible to evenly light the cone for increasing distance. Because of this effect the cone was kept in small distance to the exit of the lens tube, approximately 5 cm. In an effort to decrease the inhomogeneity nevertheless a piece of sandwich paper, picture b) in Fig. 3.4, was inserted after the LED, using two retaining rings.

Now a picture was taken with the CCD sensor without the lens system. The CCD was positioned to picture a part slightly off center with the biggest inhomogeneities that could be seen with the naked eye. Fig. 3.10 a) shows this picture. The sandwich paper succeeds in increasing the lights homogeneity. This becomes evident by comparing Fig. 3.10 a) with Fig. 3.8 a). Fig. 3.10 illustrates the bright bezel, that is far brighter than the inhomogeneities. From the intensities, measured at the center of the light spot, the mean and standard deviation were calculated:

$$mean = 183.57\text{arb u} \qquad std = 2.524\text{arb u} \tag{3.1}$$

This allowed to calculate the relative error, which is a statistical error on the light homogeneity and will be of importance for the PDE measurement:

$$\frac{\sigma_{homogeneity}}{PDE(\theta)} = 0.0137 \tag{3.2}$$

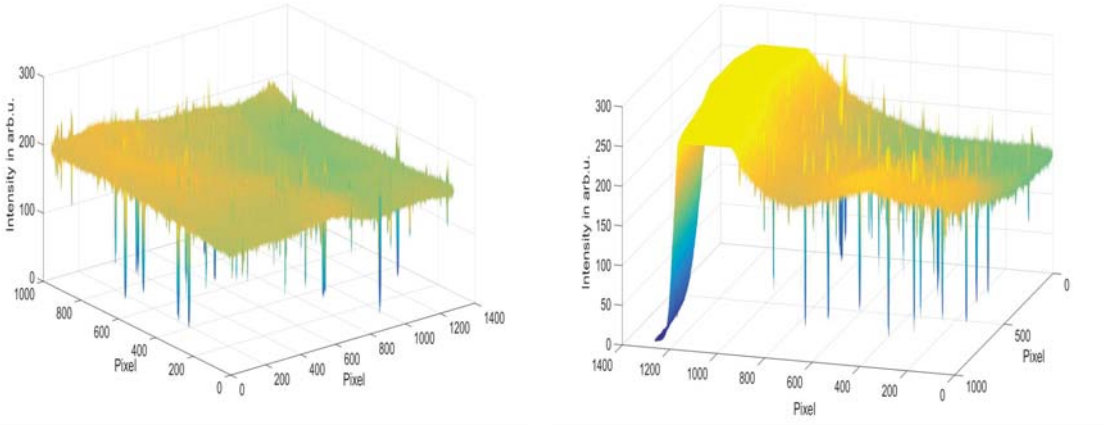

(a) (b)

Figure 3.10: a) Shows the intensities in the center of the light circle. The mean and standard deviation of these were calculated for the relative error on the light intensity. b) Shows an example of how the bright bezel is much more intense than the illuminated spot.

3.2.3 Stepper motor calibration

As the stepper motor is controlled by the arduino uno micro controller board, it makes "interleave" steps. Doubling the originally possible number of steps per revolution, utilising the two coils of the stepper motor.
To verify that the motor indeed would make 400 steps per revolution, a C++ program was developed, that made 600 interleave steps. At every step the setup would trigger 20 light pulses. Each SiPM response to the light pulse is integrated. From these values the mean and standard deviation are calculated for each step.

The pulses of the SiPM should be highest when facing the light source with the smallest entrance angle. Fig. 3.11 shows the motor callibration measurement. Marked are the two center points of the peaks. This peaks should represent the position where the Winston cone faced the light with angle $\theta = 0°$. One full revolution consecutively should be the difference in steps between the two maximum positions. The difference between these positions is 399 steps. It can therefore be calculated :

$$\frac{360°}{399} = 0.902° \tag{3.3}$$

This allows to calculate the intensity in regards to the angle θ. Furthermore it gives an absolute position for the cone to face the light source. This value complies with the doubled number of steps per revolution by the manufacturer.

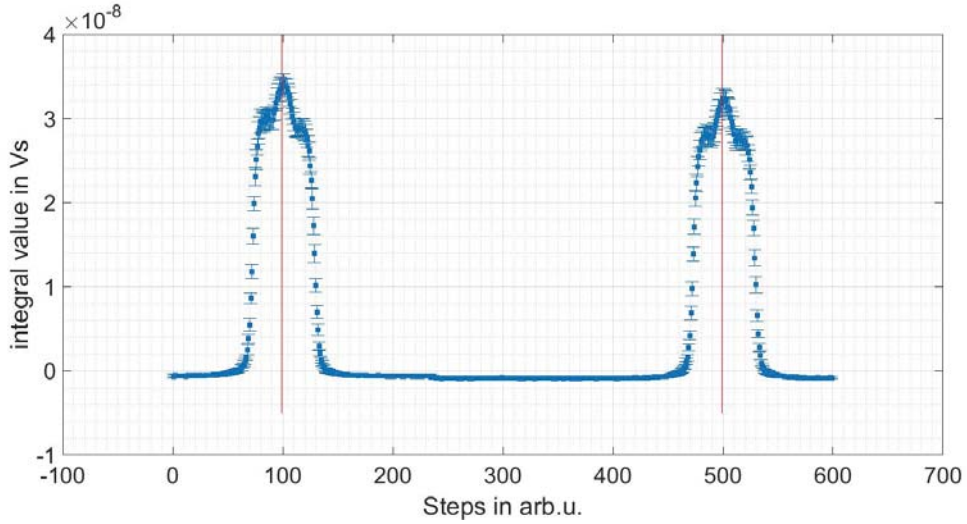

Figure 3.11: The motor calibration measurement. Shown are the mean integral values, of 20 light pulses seen by the SiPM, per step. Two peaks are visible where the cone faced the light.

3.2.4 Overvoltage

To measure the overvoltage of the SiPM the following was done: The normal bias voltage of 70.81 V was applied. The cone was facing directly in the light and the pulser was supplying the LED with the maximum possible voltage. Then the bias voltage was reduced in steps of 10 mV. Consecutively the SiPM pulses got lower. When the pulses disappeared at $V_{bias} = 69.51\,V$ the bias voltage must have fallen below the breakdown voltage. The overvoltage followed as:

$$V_{overvoltage} = V_{bias} - V_{breakdown} = 70.81\,V - 69.51\,V = 1.30\,V \tag{3.4}$$

3.2.5 Temperature monitoring

While performing the measurements the temperature in the dark box was monitored. This was done using a second arduino uno. The temperature in the room, where the measurements were performed, was regulated by an air conditioning system during the day. The SiPM's gain is temperature dependent. For increasing temperatures the measured signal will decrease. The temperature sensor allowed for a precision of ±1.4K. This uncertainty translates to a systematic error. The relative error of the SiPM's gain is given by [3], assuming a 54 mV/K progression of the overvoltage at a fixed bias voltage.

$$\sigma^{rel.}_{Temp} = 0.04\,K^{-1} \tag{3.5}$$

During the PDE measurement no temperature flux higher than the measurement uncertainty σ_{Temp} could be observed. Therefore the uncertainty on the PDE due to the temperature is:

$$\frac{\sigma_{Temp}}{PDE} = 1.4\,\mathrm{K} \cdot 4\,\% = 5.6\,\% \tag{3.6}$$

3.2.6 Crosstalk and dynamic range

A measurement was carried out to get an estimate of the crosstalk effect of the SiPM. The crosstalk effect has been explained above and refers to multiple photon pulses in the SiPM in an event of a single photon hitting the sensor or a thermal noise trigger. To estimate the probability for a crosstalk event the SiPM was isolated in the dark box with all light sources turned off. The front-end electronic is replaced by electronic dedicated for crosstalk measurements. The new electronic cuts of the long SiPM flank to 5 ns FWHM. This deals with the problem of two separate pulses in a short time window stacking together. The remaining chance for a second event in the short pulse width can be estimated with following equation from [3]:

$$p_{2ndevent} = (1 - e^{-f_{darknoise} \cdot \Delta t}) \tag{3.7}$$

With a darknoise rate of 12 MHz and a time of $\Delta t = 5$ ns the resulting chance for a second event is:

$$p_{2ndevent} = 0.0582 \tag{3.8}$$

Comparing this to the 100 ns pulses of the other electronic, the error on the measured rates is greatly reduced. The trigger of the oscilloscope was now altered in two steps.

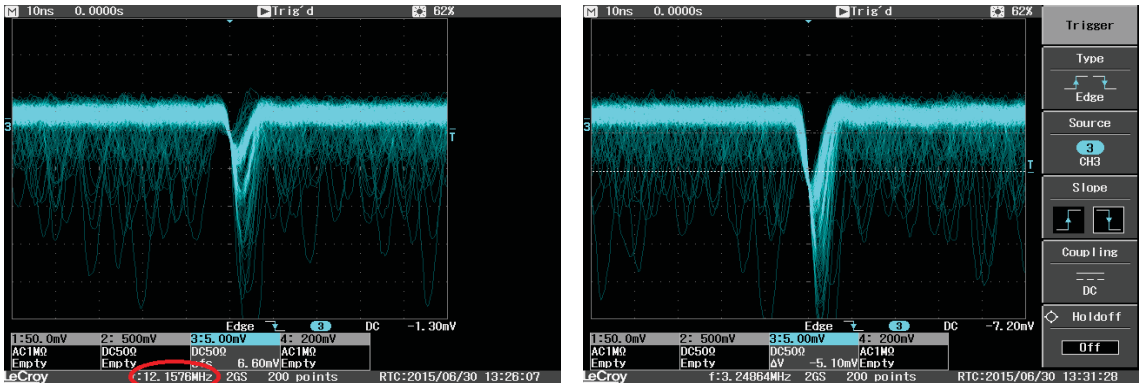

(a) (b)

Figure 3.12: Two screenshots of the oscilloscope with different trigger levels. a) at about 0.5 p.e. b) about 1.5 p.e. . The oscilloscope directly measures the trigger rate. Highlighted in a) is the trigger rate measured by the oscilloscope.

First the trigger was set to trigger at approximately 0.5 p.e. $\cong -1.3\text{mV}$. This way all events larger than 0.5 p.e. should be triggered. This is shown in Fig. 3.12 a). In the next step the trigger level was increased to approximately 1.5 p.e. $\approx -7.2\text{mV}$. This is shown in 3.12 b). Multiple measurements were performed and the mean of the measured rates calculated.

$$f_{0.5pe} = 3.11 \pm 0.04\,\text{MHz} \tag{3.9}$$

$$f_{1.5pe} = 12.18 \pm 0.09\,\text{MHz} \tag{3.10}$$

Combining (3.9) and (3.10) we can estimate the chance for a crosstalk event. Because all events with 2 p.e. or more are estimated to be caused by crosstalk.

$$p_{crosstalk} = \frac{3.11 \pm 0.04\text{MHz}}{12.18 \pm 0.09\text{MHz}} = 0.2553 \pm 0.072 \tag{3.11}$$

This crosstalk probability does not account for the number of photons that are created on a photon event though, as the trigger of 1.5 p.e. includes higher numbers. To get an understanding of the real number of photons detected depending on the number of incoming photons the following simulation was written:
A 3600 cell SiPM was simulated. Single p.e. events were forced on the SiPM, triggering a cell. With the crosstalk probability of approximately 25%, there was an assumed chance of $\frac{25\%}{8} = 3\%$ for each of the eight neighbouring cells to trigger. Each of these cells again could trigger crosstalk events in their neighbouring cells and so on.

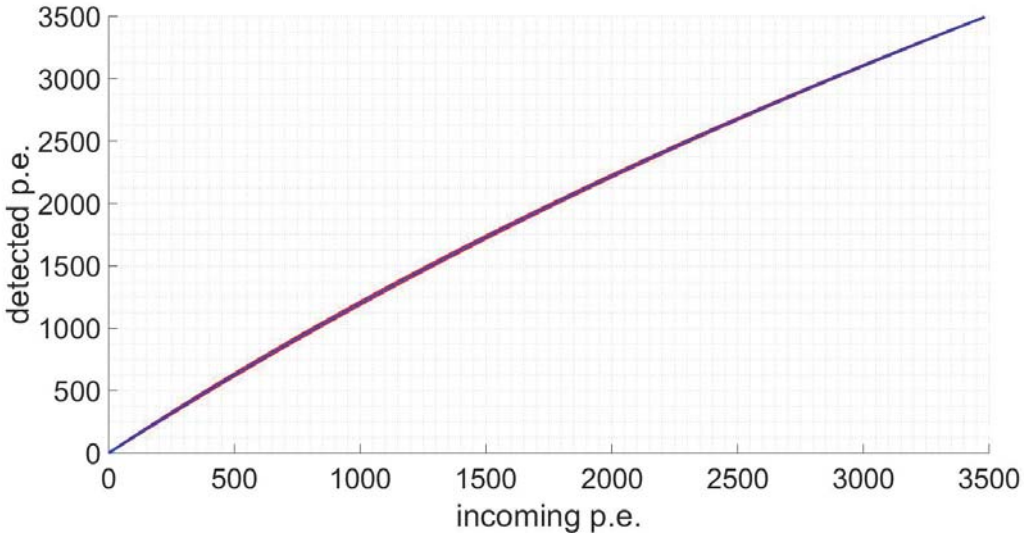

Figure 3.13: Shown are the simulated numbers of crosstalk photoelectrons depending on the number of real p.e.. It shows that the number of detected p.e. does not rise linear with increasing incoming p.e.. The slight decrease for higher incoming p.e. is due to the limited number cells, i. e. the dynamic range of the SiPM.

There was no time of flight for the crosstalk photons. Cells that triggered already could not trigger a second time. The number of forced p.e. was consecutively increased, resulting in a function of measured photoelectrons of real detected photoelectrons. This is shown in Fig. 3.13. This result was parametrized and will be used to correct the PDE simulation and measurement for crosstalk.

Because this simulation only allows a cell to trigger once, the whole simulation process is instantaneous. This means that the simulation also incorporates the dynamic range of the SiPM. Therefore when using the parametrised function to correct the simulation or measurement, it should not only correct for the crosstalk but also for the dynamic range effect.

4. Photon detection efficiency

The photon detection efficiency is defined by (1.1) on page 2. For the combined PDE of SiPM and Winston cone the absorption of the aluminium will have a high impact. Because light going into the cone, with a bigger distance to the optical axis, will be reflected on the walls of the cone more often, it has a higher chance of being absorbed. Combining this with the angular dependent $PDE_{SiPM}(\theta)$, found in [7] and shown in Fig. 2.4 on page 7, equation (1.1) is altered:

$$PDE_{combined}(\theta) = PDE_{SiPM} \cdot PDE_{WiCo} \cdot PDE_{SiPM}(\theta) \cdot PDE_{WiCo}(\theta) \tag{4.1}$$

Because the goal is a relative PDE measurement the non angular dependent parts of (4.1) will cancel each other out:

$$PDE^{rel}_{combined}(\theta) = \frac{PDE_{WiCo}(\theta) \cdot PDE_{SiPM}(\theta)}{PDE_{WiCo}(0°) \cdot PDE_{SiPM}(0°)} \tag{4.2}$$

This also lessens the effect of the measurement error due to crosstalk. By dividing the PDE by $PDE(0°)$, which includes this crosstalk events, most additional cross talk events will cancel out. To get an understanding of $PDE_{WiCo}(\theta)$ a simulation was programmed.

4.1 Simulation of the relative photon detection efficiency

The simulation was written in Matlab 2014b. It defines only the two dimensional shape of the Winston cone. Then photons enter, with a angle θ to the optical axis, and traverse through the cone. Their path is tracked. If they hit the aluminium there is a 6% chance they are absorbed, in accordance to [9]. If not they are reflected according to Snell's law.

Matlab's uniform random number generator is used to generate starting positions for photons in the entrance plane of the cone. These photons travel in the direction given by the entrance angle θ and, if they reach the exit plane of the cone, are counted and their exit angle is stored.

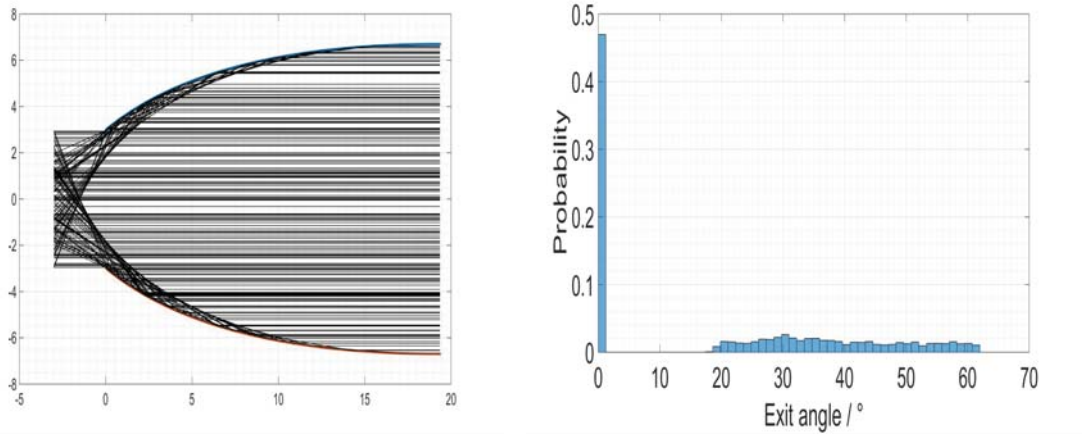

(a) (b)

Figure 4.1: a) Simulation of 200 photons reflecting inside the Winston cone. Entrance angle $\theta = 0°$b) Histogram of the exit angles of 5000 simulated photons.

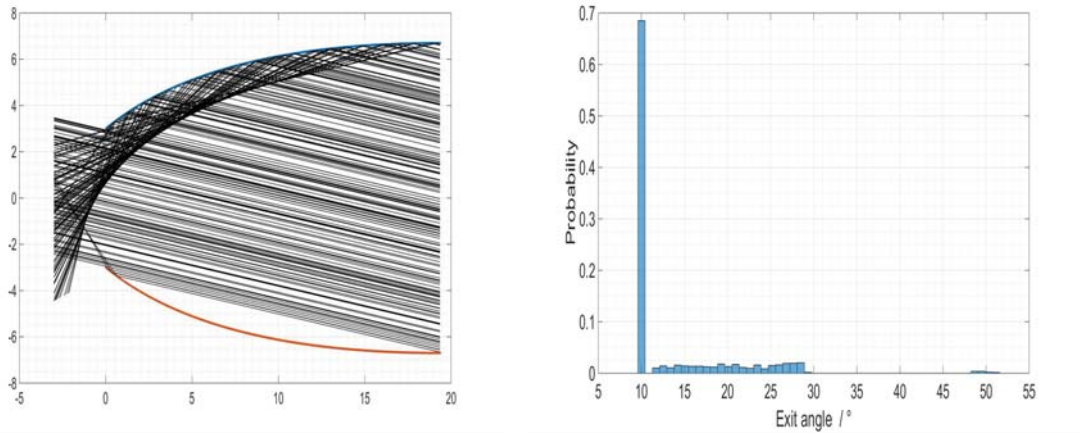

(a) (b)

Figure 4.2: a) Simulation of 200 photons reflecting inside the Winston cone. Entrance angle $\theta = 10°$b) Histogram of the exit angles of 5000 simulated photons.

Figures 4.1, 4.2 and 4.3 show how 200 photons reflect inside the cone and exit through the exit aperture. The histograms show the exit angles of 5000 photons with the corresponding entrance angles. For high entrance angles the exit angles also increase. This has a high impact because of the angular dependent PDE of the SiPM. The PDE of SiPM and Winston cone is expected to lower towards higher entrance angles.

To get an understanding of the overall PDE of SiPM and Winston cone a simulation was performed that folded the exit angles with the angular dependent PDE shown in Fig. 2.4 on 7. The plot in Fig. 2.4 was parametrised with an exponential function and folded with the exit angles of the photons in the simulation.

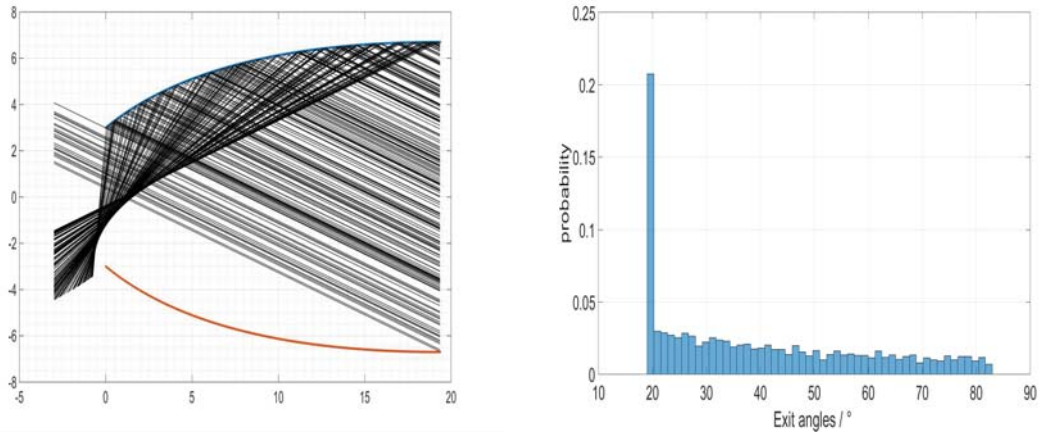

(a) (b)

Figure 4.3: a) Simulation of 200 photons reflecting inside the Winston cone. Entrance angle $\theta = 20°$b) Histogram of the exit angles of 5000 simulated photons.

The simulation was performed in steps of 0.5°for the entrance angle θ. At each position 2000 photons were simulated. The exit angles to the optical axis at $\theta = 0°$ were folded as explained. The simulation was also modified with the function obtained from the simulation for crosstalk and the dynamic range of the SiPM.

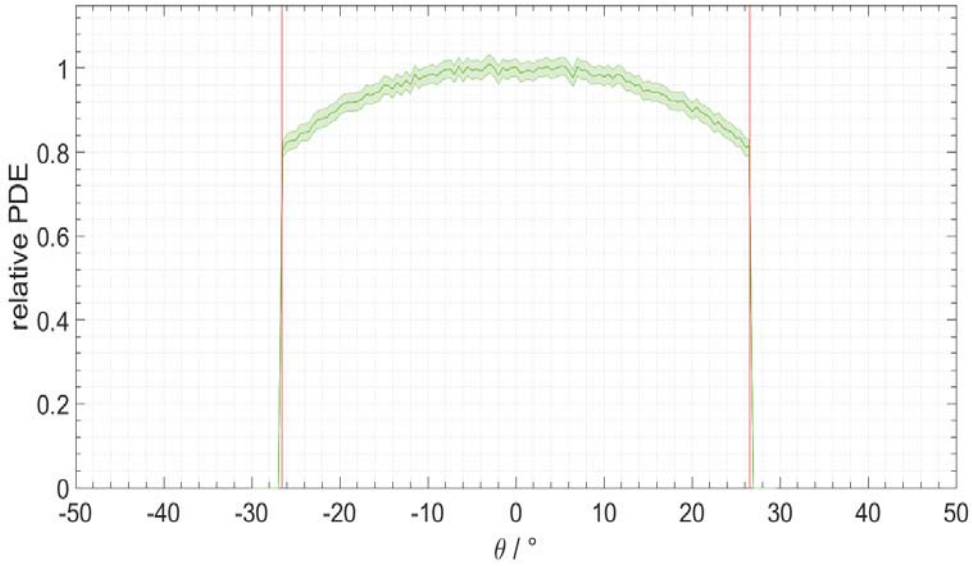

Figure 4.4: PDE simulation folded with the angular dependent PDE of the SiPM. Also weighted with $\cos\theta$ to account for the three dimensional loss of illuminated area with increasing θ. The simulated PDE falls as expected with increasing θ. The simulation is modified for the effects of crosstalk.

The simulation of $PDE_{combined}(\theta)$ can be seen in Fig. 4.4. It falls as expected with increasing θ. The folded PDE values were weighted with $\cos\theta$ to account for

the decrease in illuminated area with increasing θ. For the uncertainty a Poisson distribution was estimated resulting in a Poisson error $\sqrt{N}$. This is incorporated in the simulation of 2000 photons per 0.5°trough

$$\sigma_{Simu.} = \sqrt{2000 \cdot PDE_{simulated,folded}(\theta)} \tag{4.3}$$

While for a perfect Winston cone without absorption and the effect of the SiPM a square shape with $PDE(\theta) = 1$ for θ in $[-\theta_{max}, \theta_{max}]$ would be expected, we see that the PDE decreases by about 25% towards θ_{max} in Fig. 4.4.As expected with entrance angles above θ_{max} no light leaves the cone through the exit aperture.
The simulation does not however account for some effects, like the round shape of the Winston cone on the squared surface of the SiPM package, not perfectly sharp edges of the material and no three dimensional representation of the cone. Better simulations written by T. Niggemann in [4] show that the hard cut off for θ_{max} softens when taking additional effects into account.

4.2 Main measurement and analysis

4.2.1 Measurement

The main measurement was now performed with the setup of the former chapter. 50 light pulses were evaluated per motor step. The PDE is the combined PDE of SiPM and Winston cone:

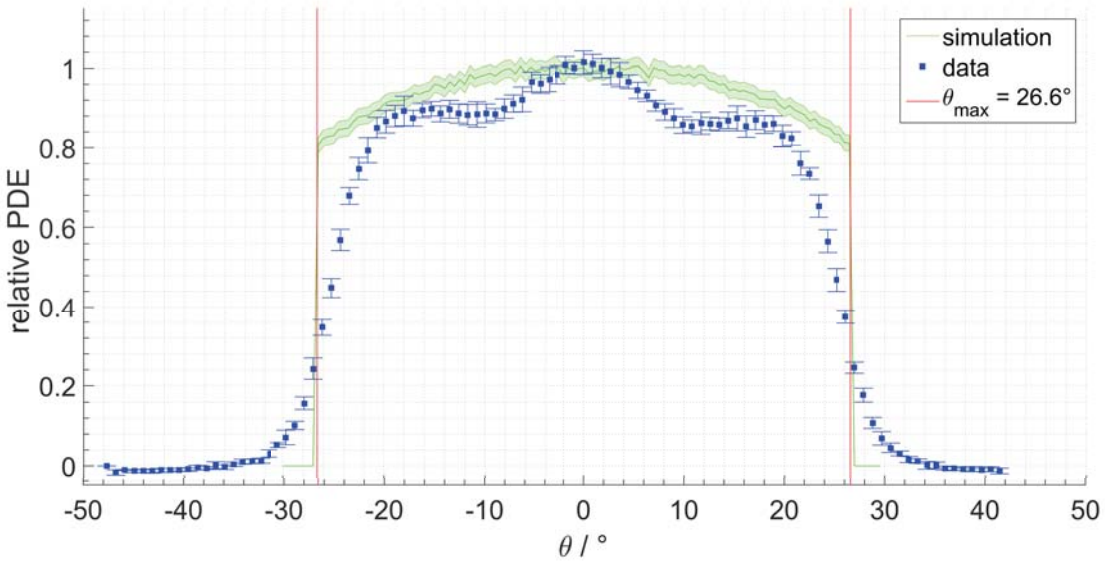

Figure 4.5: The PDE measurement in blue. The PDE is highest at $\theta = 0°$. After a fall of it reaches a plateau at about $\theta = \pm 12°$. Towards $\theta = \theta_{max}$ it falls steep and reaches 0 at $\theta = 35°$. The simulation has been corrected for crosstalk and dynamic range effects.

In Fig. 4.5 we see the PDE measurement performed, combined with the simulation which has been corrected for crosstalk and dynamic range. The PDE has its maximum at $\theta = 0°$. With increasing θ the intensity first falls faster than simulated until roughly $\theta = \pm 10°$. There it stabilises at 0.8 until $\theta = \pm 20°$, where it nearly matches the simulated PDE. With further increasing θ the PDE falls steeply.At 25° the PDE had reached 50 %. At $\theta = \pm\theta_{max}$ the PDE has reached about 25%. At $\theta = \pm 35°$ the PDE is 0.
A new maximum entrance angle was chosen, by calculating the slopes and choosing the angle with the highest slope $\tilde{\theta}_{max,1} = -24.3 \pm 0.5°$ and $\tilde{\theta}_{max,2} = 26.1 \pm 0.5°$. Their mean was calculated:

$$\tilde{\theta}_{max} = 25.2 \pm 0.35° \tag{4.4}$$

This value does not deviate far from the theoretical value for $\theta_{max} = 26.6°$. The Winston cone fulfils its designated purpose.

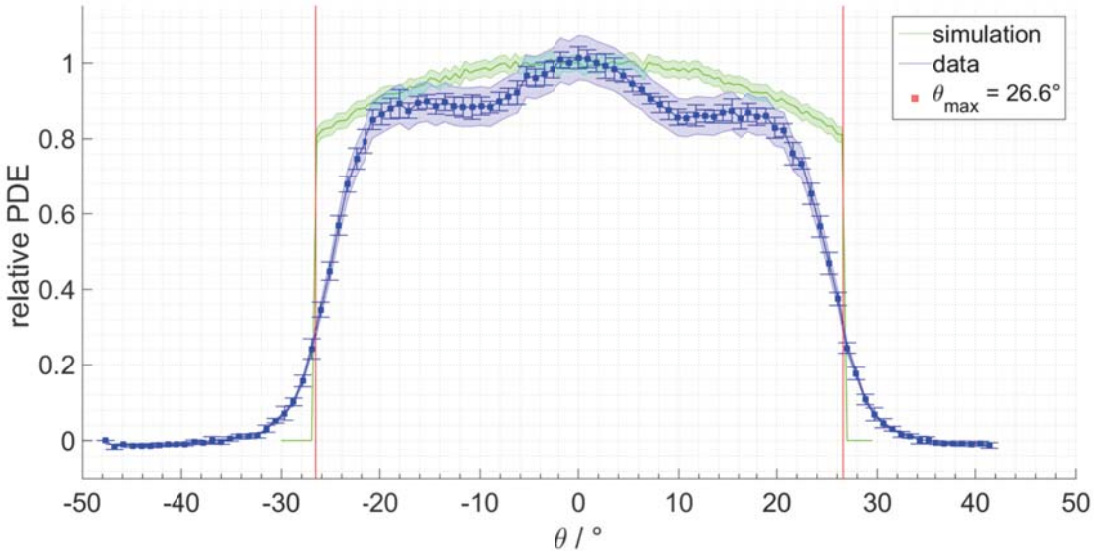

Figure 4.6: The PDE measurement. The systematic errors have been plotted as a shaded blue area. The two parts of this error are $\sigma_{homogeinity}$ and $\sigma_{Temp.}$. With this errors the simulation and the measured data overlap around $\theta = 20°$.

Fig. 4.6 shows the measurement with the combined error of light homogeneity and temperature shown as a shaded error band. The simulation has two major shortcomings: The softened falloff at $\theta = 26.6°$ can not be found in this simulation. It seems to appear though in a more precise simulation. Like the ones done by T. Niggemann in [4]. Second, while the simulation comes close to the measured values at $\theta = 0°$ and at about $\theta = \pm 20°$, in between the measured values form "dips". These "dips" were reproduced on all measurements. In the next section an effort was made to understand the reason for the loss of PDE in this angle area.

For easy parametrisation the mean of the measured data of an entrance angle was calculated $PDE_{mean} = \frac{PDE(\theta)+PDE(-\theta)}{2}$. These new PDE values were corrected for

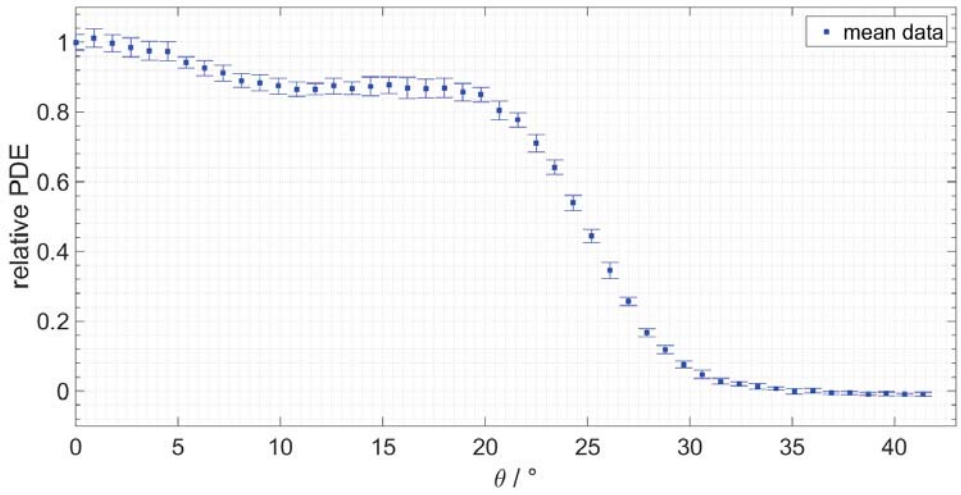

Figure 4.7: The mean of the measured PDE data for $\pm\theta$. The mean values are corrected for crosstalk and dynamic range effects with the simulation mentioned above.

crosstalk and dynamic range effects. The plot of PDE_{mean} against θ is shown in Fig. 4.7. The data for this plot is available in the appendix A.3.

4.2.2 Analysis

To estimate the PDE loss the simulation and the measurements values were summed respectively from $\theta = 0°$ to $\theta = 20°$. The sum of values of the simulation was divided by the sum of values of the measurements:

$$\frac{\Sigma_{simu.}^{0-20}}{\Sigma_{measu.}^{0-20}} = 1.0409 \tag{4.5}$$

This means approximately 4% of the expected light is lost in this angular range. Two effects were considered in an attempt to explain these dips:
Estimating the absorption of the photons reflecting at the aluminium cone with a flat 6% might have been to imprecise. The reflection and transmission of the photons is given by the Fresnel equations and the complex refractive index of the aluminium, which also is wavelength dependent. In his thesis [9] S. Mann chose this refractive index for light with wavelength $\lambda = 400\text{nm}$

$$\tilde{n_2} = 0.4879 + 4.855i \tag{4.6}$$

The refractive index of air is $n_1 = 1$. The Fresnel equations for perpendicular polarised light R_s and for parallel polarised light R_p [9] .

$$R_s = \left| \frac{\tilde{n}_1 \cos\theta - \tilde{n}_2 \sqrt{1 - (\frac{\tilde{n}_1}{\tilde{n}_2} \sin\theta)^2}}{\tilde{n}_1 \cos\theta + \tilde{n}_2 \sqrt{1 - (\frac{\tilde{n}_1}{\tilde{n}_2} \sin\theta)^2}} \right|^2 \tag{4.7}$$

$$R_p = \left| \frac{\tilde{n}_1 \sqrt{1 - (\frac{\tilde{n}_1}{\tilde{n}_2} \sin\theta)^2} - \tilde{n}_2 \cos\theta}{\tilde{n}_1 \sqrt{1 - (\frac{\tilde{n}_1}{\tilde{n}_2} \sin\theta)^2} + \tilde{n}_2 \cos\theta} \right|^2 \tag{4.8}$$

Because the light from the LED is unpolarised, the equations were combined:

$$R = \frac{R_s + R_p}{2} \tag{4.9}$$

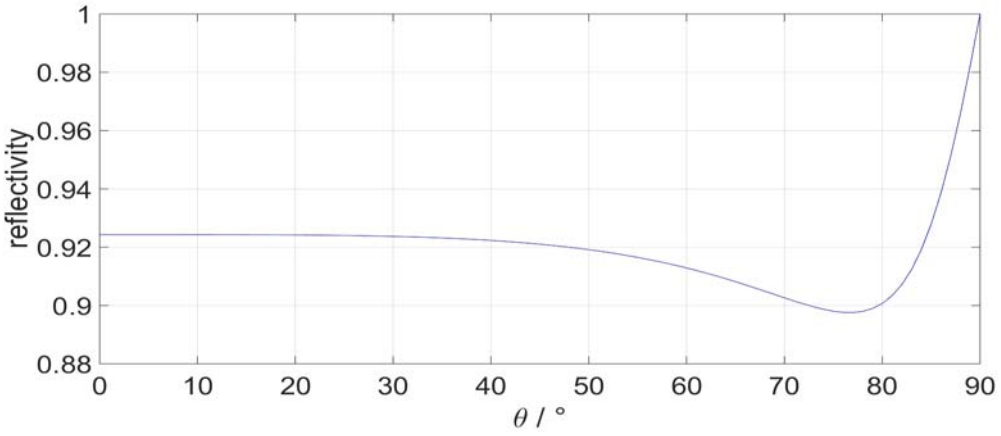

Figure 4.8: Angle dependent reflectivity of aluminium for light with $\lambda = 400$nm. The shape of the function differs greatly from a flat value.

The resulting reflectivity in dependence of the entrance angle θ is shown in Fig. 4.8. This function was implemented in the simulation.

The second effect estimated was the idea of a non perfect cone end. In the simulation the cone end is a perfect line with no width. In reality the cones are milled from a solid aluminium piece. The idea was, that the finite width of the aluminium with a rounded shape at the exit aperture makes light that enters the cone with a high angle θ close to θ_{max} reflect and exit the cone with a low angle. Considering that the angular dependent PDE of the SiPM falls of for high angles a behaviour similar to the measurement data was expected.

The round ending was estimated as a parabola with a width of 0.1 mm. The Shape can be seen in Fig. 4.9 b). As was shown in Fig. 4.3, the photons concentrate in a quite a narrow beam for high entrance angles. If this beam hits the round edge shown Fig. 4.9 the light should emit with angles close to $\theta = 0°$.

These two effects were implemented in the simulation. Because of the increased complexity and time constraints only 500 photons/0.5° were simulated.

The new simulation is shown in Fig. 4.10 in comparison with the measurement data. Sadly not only does the simulation not comply with the ”dips”, it even shows

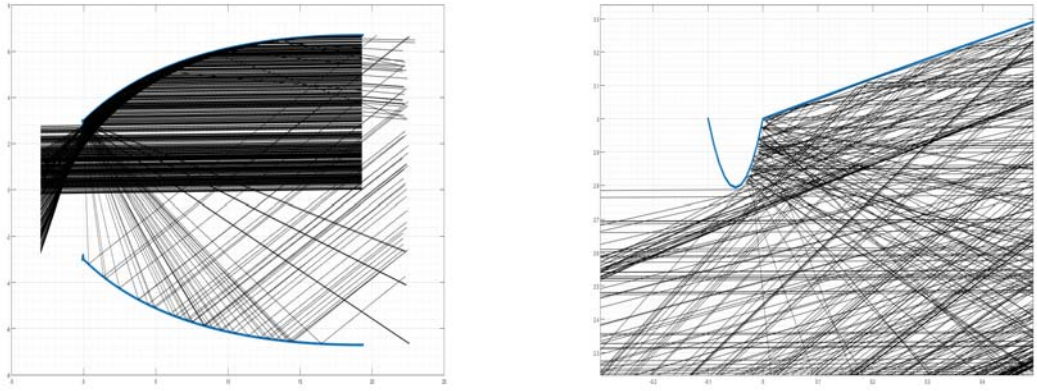

(a) **(b)**

Figure 4.9: The plots show the simulation of a round ending of the Winston cone. The ending was estimated with a parabola shape with a width of 0.1mm. a) 500 Photons starting in the upper half of the cone reflect on the cone and the round ending. Photons reflecting at the round ending do not reach the SiPM. b) Shows the estimated parabola shape of the round ending.

an opposite effect than expected, the simulated PDE increases in the angle range of $\theta = 0..20°$. It is possible that three dimensional effects or effects of the lobed surface of the cone create these dips. Due to the complexity of such a simulation, it was not possible to include these features in the simulation described here.

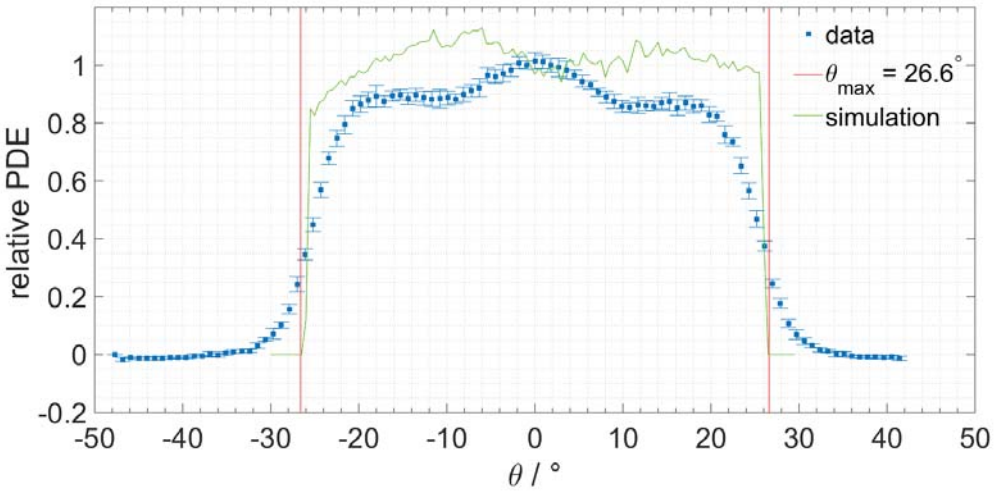

Figure 4.10: The plot shows the measurement data in blue. The new simulation with both effects discussed above is shown in green. The simulation was modified with the crosstalk function obtained earlier. The simulation does not comply with the measurement data. It fails to show the "dips" in the range of $\theta = 0..20°$.

5. Conclusion

5.1 Winston cones in the FAMOUS telescope

The photon detection efficiency of the Winston cones of the FAMOUS telescope was successfully measured. The designed experimental setup proved to be suitable and stable. The Winston cones fulfil their desired role. They cut out the light at a entrance angle

$$\tilde{\theta}_{max} = 25.2 \pm 0.35\,^{\circ} \tag{5.1}$$

while increasing the light sensitive area. The value found for θ_{max} deviates slightly from the theoretical prediction, does depend on the definition of θ_{max} though. If θ_{max} is chosen for an intensity of 25% of the intensity at $\theta = 0°$ the value seems to correspond with the theoretical value quite well. The written simulation does fall short though. It does not account for an approximately 4% light loss, which could not be explained by including the angular dependent reflectivity given by the Fresnel equations and the rounded edges of the Winston cone exit aperture. A different and maybe more complex shape could provide a solution. Because the FAMOUS telescope might utilise different SiPMs in its final version, if angular dependent PDE measurements were performed for them, they can easily be incorporated into the simulation. This allows to easily compare to a then measured PDE.

5.2 Winston cones in other applications

During the work on the thesis the opportunity arose to help in applications of Winston cones. The Pierre Auger collaboration plans to upgrade the observatory with detectors suited for measuring the muonic component, the SiPM group at RWTH Aachen university proposed a scintillator read-out with SiPMs. These modules which have already been shipped to Argentina and which will be deployed in several stations this week, utilise solid simplified Winston cones to concentrate light from a bundle of optical fibres onto a SiPM. These cones are no real Winston cones because they don't follow a parabolic shape. Nevertheless they can put to great use as light concentrators. To get a quick understanding of the way the cone shapes the light and the homogeneity of the light exiting the simplified cone, some pictures were taken with the CCD camera.

Fig. 5.1 shows a picture of the light leaving the simplified cone. The light shows a clear pattern, that was dependent on the positions of the optical fibres on the

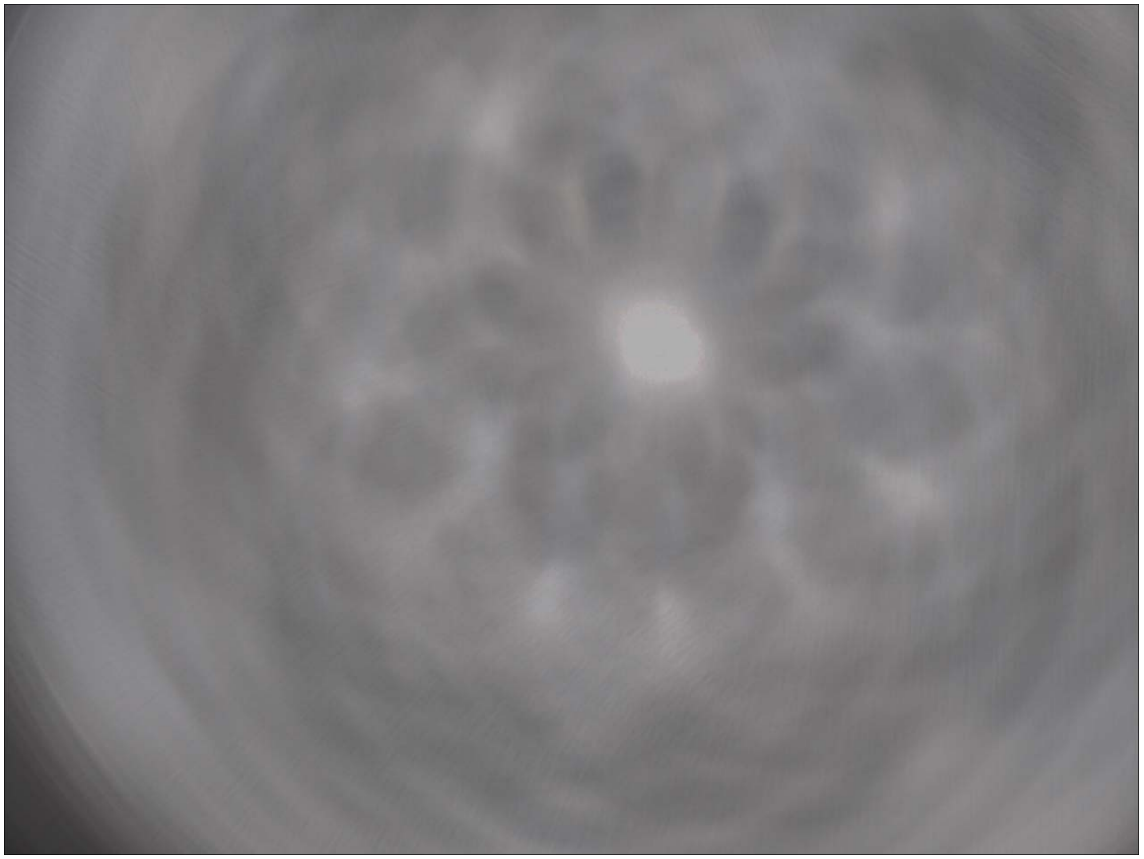

Figure 5.1: The picture shows the light leaving the simplified solid cone. A clear pattern is visible. The light will not illuminate the SiPM homogeneously.

entrance of the cone. This pattern could be important when considering the dynamic range of the SiPM in this application. As the SiPM is not illuminated evenly some areas may saturate while others see hardly any light.

Winston cones or simplified versions have a great area of application in telescopes. Like already in use in the Pierre Augers FD telescopes or in the First G-APD cherenkov telescope (FACT) [12] they are an easy to produce and efficient way to increase light sensitive area. The possibility to produce hollow ones minimising absorption and their ability to be easily maintained further speak in their favour.

A. Appendix

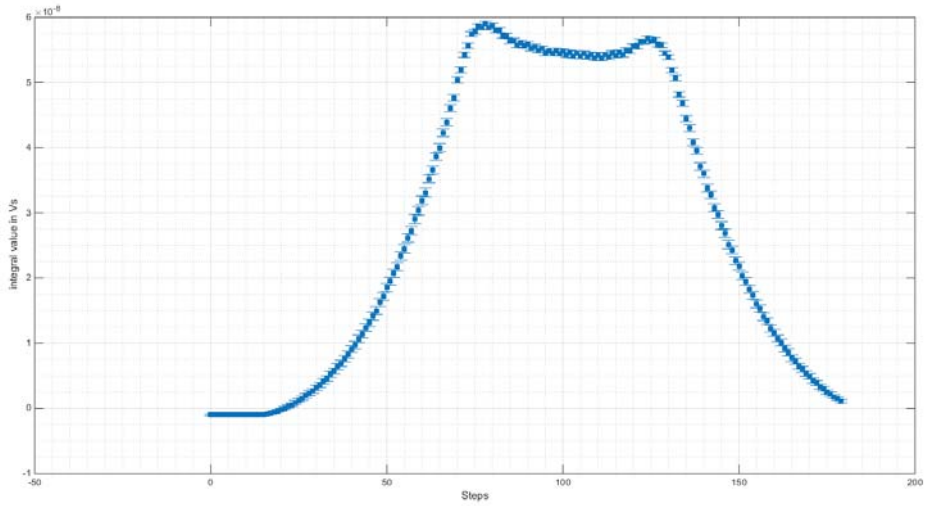

Figure A.1: Shown is an early measurement, where the measured charge is plotted against the motor steps. The expected PDE structure is visible, but dominated by small "horns" towards the maximum entrance angle. This measurement was performed with the SiPM being fixed in the notch of the Winston cone with 2 metal clamps made of wire. Once these clamps were removed and the SiPM was glued into the notch of the Winston cone, these "horns" disappeared. It was concluded that they are appear due to reflection in a small cavity between the SiPM and the Winston cone.

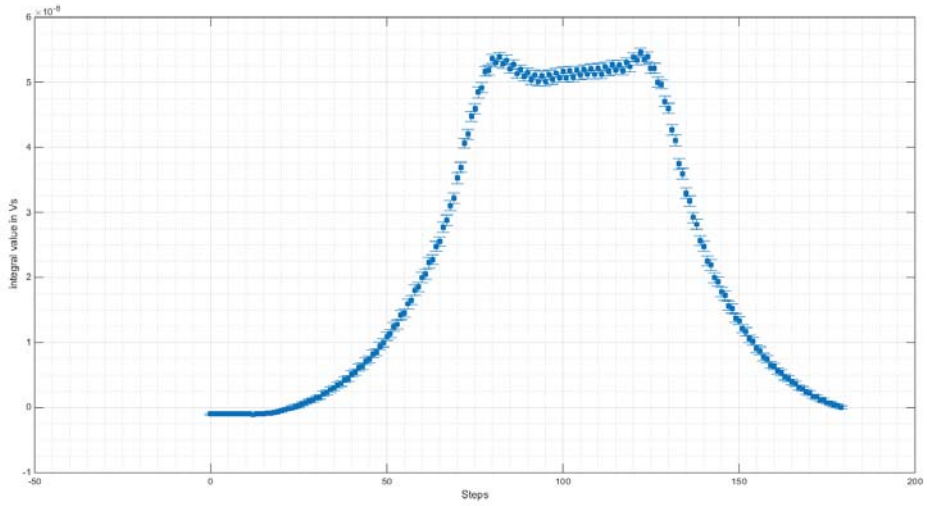

Figure A.2: Again a measurement where two ”horns” are visible. Also a overall slope in the measured integral values is evident. This slope appeared when the Winston cone was not positioned exactly centred in the light beam. Another visible effect are that the integral values seemed to jump in pairs of two. This was due to the stepper motor being operated in interleave mode. In this mode the motor drains double the current than listed. If not provided with such an amount of current (850 mA)the motor alternated between small and bigger steps, still covered the same range though.

Theta	sigma_theta	rel. PDE	sigma_stat	sigma_sys
0,0000	0,0023	1,0000	0,0052	0,0577
0,9000	0,0023	1,0118	0,0037	0,0583
1,8000	0,0023	0,9973	0,0058	0,0575
2,7000	0,0023	0,9852	0,0041	0,0568
3,6000	0,0023	0,9754	0,0047	0,0562
4,5000	0,0023	0,9736	0,0041	0,0561
5,4000	0,0023	0,9418	0,0063	0,0543
6,3000	0,0023	0,9252	0,0078	0,0533
7,2000	0,0023	0,9113	0,0045	0,0525
8,1000	0,0023	0,8903	0,0080	0,0513
9,0000	0,0023	0,8838	0,0061	0,0510
9,9000	0,0023	0,8742	0,0087	0,0504
10,8000	0,0023	0,8650	0,0116	0,0499
11,7000	0,0023	0,8654	0,0098	0,0499
12,6000	0,0023	0,8745	0,0115	0,0504
13,5000	0,0023	0,8677	0,0117	0,0500
14,4000	0,0023	0,8735	0,0116	0,0504
15,3000	0,0023	0,8764	0,0236	0,0505
16,2000	0,0023	0,8690	0,0190	0,0501
17,1000	0,0023	0,8678	0,0217	0,0500
18,0000	0,0023	0,8696	0,0207	0,0501
18,9000	0,0023	0,8563	0,0248	0,0494
19,8000	0,0023	0,8498	0,0207	0,0490
20,7000	0,0023	0,8042	0,0265	0,0464
21,6000	0,0023	0,7770	0,0203	0,0448
22,5000	0,0023	0,7099	0,0253	0,0409
23,4000	0,0023	0,6412	0,0277	0,0370
24,3000	0,0023	0,5394	0,0266	0,0311
25,2000	0,0023	0,4450	0,0300	0,0257

Figure A.3: Mean PDE values for $\pm\theta$. They are corrected for crosstalk.

26,1000	0,0023	0,3455	0,0239	0,0199
27,0000	0,0023	0,2572	0,0268	0,0148
27,9000	0,0023	0,1669	0,0180	0,0096
28,8000	0,0023	0,1192	0,0228	0,0069
29,7000	0,0023	0,0765	0,0167	0,0044
30,6000	0,0023	0,0478	0,0205	0,0028
31,5000	0,0023	0,0279	0,0231	0,0016
32,4000	0,0023	0,0203	0,0224	0,0012
33,3000	0,0023	0,0126	0,0199	0,0007
34,2000	0,0023	0,0076	0,0232	0,0004
35,1000	0,0023	-0,0010	0,0220	-0,0001
36,0000	0,0023	0,0015	0,0162	0,0001
36,9000	0,0023	-0,0054	0,0272	-0,0003
37,8000	0,0023	-0,0056	0,0271	-0,0003
38,7000	0,0023	-0,0086	0,0274	-0,0005
39,6000	0,0023	-0,0083	0,0240	-0,0005
40,5000	0,0023	-0,0099	0,0263	-0,0006
41,4000	0,0023	-0,0094	0,0222	-0,0005

References

[1] T. P. A. Collaboration, *The pierre auger cosmic ray observatory*, Nuclear Instruments and Methods in Physics Research Section A: Accelerators, Spectrometers, Detectors and Associated Equipment, (2015), pp. –.

[2] Gentile, S. and Kuznetsova, E. and Meddi, F., *Photon detection efficiency of Geiger-mode avalanche photodiodes*, ArXiv e-prints, (2010).

[3] M. Lauscher, *Characterisation studies of silicon photomultipliers for the detection of fluorescence light from extensive air showers*, master's thesis, RWTH Aachen, 2012.

[4] T. Niggemann, *New telescope design with silicon photomultipliers for fluorescence light detection of extensive air showers*, master's thesis, RWTH Aachen, 2012.

[5] Hamamatsu, *MPPC (multi-pixel photon counter) New type of Si photon-counting device Array type (1 x 4 ch, 2 x 2 ch) S10984/S10985 series*.

[6] S. H. Simon, *The Oxford Solid State Basics*, Oxford University Press, 2013.

[7] D. Wilson, *Angular dependencies of the relative photon detection efficiency of silicon photomultipliers*, bachelor thesis, RWTH Aachen, September 2012.

[8] P. G. B. Roland Winston, Juan C. Minano, *Nonimaging optics*, Academic Press, 2005.

[9] S. Mann, *Measurement of the uv reflectivity of aluminium in different stages of oxidation*, bachelor thesis, RWTH Aachen, 2012.

[10] Tim Niggemann et. al., ed., *Status of the Silicon Photoultiplier Telescope FAMOUS for the Fluorescence Detection of UHECRs*, 2013.

[11] J. Schumacher, *Front-end electronics for silicon photomultipliers*, master's thesis, RWTH Aachen, 2014.

[12] Thomas Bretz et. al., *Fact - the first g-apd cherenkov telescope: Status and results*, ArXiv e-prints, (2013).

Acknowledgements

Hiermit möchte ich mich bei all denen bedanken, ohne die diese Arbeit nicht möglich gewesen wäre.

Mein erster Dank gilt Jun. Prof. Dr. Thomas Bretz, der es mir ermöglicht hat diese Arbeit zu verfassen. Weiterhin bedanke ich mich bei Prof. Dr. Thomas Hebbeker für die Möglichkeit die Arbeit am dritten physikalischen Institut A zu verfassen und dafür, dass er sich Bereit erklärt hat meine Arbeit als Zweitkorrektor mit zu bewerten.

An zweiter Stelle danke ich meinem Betreuer Johannes Schumacher, der mir in vielen Stunden zur Seite stand. Er vermittelte nicht nur immer ruhig und konzentriert Unmengen an kostbarem Wissen, sondern leistet beim Versuchsaufbau, bei der Programmierarbeit und an vielen herrausfordernden Stellen nicht nur physische und physikalische sondern auch moralische Hilfe. Vor allem in den letzten und arbeitsintensivsten Tagen bliebst du ruhig und standest mit unverzichbarer Hilfe zur Seite.

Weiterhin bedanke ich mich bei Herrn Phillips von der Mechanik Werkstatt, der für mich die Halterung des Winston cones entworfen und gebaut hat.

Auch möchte ich den Mitarbeitern des III. Physikalischen Instituts bedanken, die mich sehr nett aufgenommen haben und bei denen ich auch durch die Teilnahme an den Meetings wunderbare Einblicke ins wissenschaftliche Abeiten gewinnen konnte.

Ein großer Dank gilt meinen Freunden und meiner Familie für die moralische Unterstützung als sie am nötigsten war.

Erklärung

Hiermit versichere ich, dass ich diese Arbeit einschließlich beigefügter Zeichnungen, Darstellungen und Tabellen selbstständig angefertigt und keine anderen als die angegebenen Hilfsmittel und Quellen verwendet habe. Alle Stellen, die dem Wortlaut oder dem Sinn nach anderen Werken entnommen sind, habe ich in jedem einzelnen Fall unter genauer Angabe der Quelle deutlich als Entlehnung kenntlich gemacht.

Aachen, den 20. Juli 2015

Johannes Merz